RESEARCH ACTIVITIES V
Department of Applied Molecular Science

V-A Molecular Mechanisms of Oxygen Activation by Heme Enzymes

By sharing a common prosthetic group, the heme enzymes such as cytochrome P450s, peroxidases, and catalases catalyze their own unique biological functions; monooxygenation, hydrogen peroxide dependent oxidation, and dismutation of hydrogen peroxide, respectively. Our efforts have been focused on the elucidation of the structure-biological function relationship of those heme enzymes by employing both enzymic systems including mutants and their model systems.

V-A-1 On the Formation and Reactivity of Compound I of the His64 Myoglobin Mutants

Toshitaka MATSUI, Shin-ichi OZAKI and Yoshihito WATANABE

[*J. Biol. Chem.* **272**, 32735 (1997)]

Myoglobin (Mb) catalyzes various two-electron oxidations; however, ferryl porphyrin cation radical equivalent to peroxidase compound I has not been identified yet. Distal histidine mutants of sperm whale Mb (His-64 → Ala, Ser and Leu) afford an apparent intermediate followed by the formation of a ferryl heme (Mb-II) in the reaction with *m*-chloroperbenzoic acid (*m*CPBA) (Figure 1). Since the intermediate exhibits characteristic absorption spectrum of compound I and bears two electron oxidizing equivalents above the ferric state, we have assigned the species as compound I of myoglobin (Mb-I). Although we have recently observed compound I of the F43H/H64L Mb mutant, F43H and wild type Mb react with *m*CPBA to give Mb-II without any accumulation of Mb-I. The results unambiguously indicate that His-64 plays a key role in destabilizing wild type Mb-I. Furthermore, Mb-I is found to be capable of performing two-electron oxidation of styrene, thioanisole and H_2O_2.

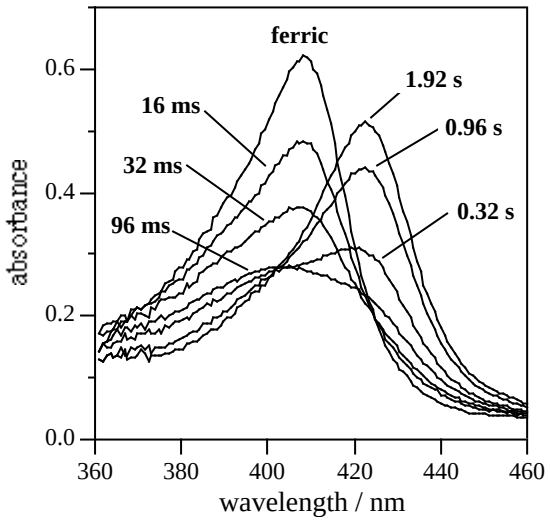

Figure 1. Time dependent spectral changes in the reaction of H64A Mb with *m*CPBA at 5.0°C in 50 mM sodium phosphate buffer, pH 7.0.

V-A-2 Effects of the Location of Distal Histidine in the Reaction of Myoglobin with Hydrogen Peroxide

Toshitaka MATSUI, Shin-ichi OZAKI and Yoshihito WATANABE

[*J. Biol. Chem.* in press]

In order to clarify how the location of distal histidine affects on the activation process of H_2O_2 by heme proteins, we have characterized reactions with H_2O_2 for L29H/H64L and F43H/H64L mutants of sperm whale myoglobin (Mb) designed to locate the histidine farther from the heme iron. While the L29H/H64L double substitution retards the reaction with H_2O_2, an 11-fold rate increase *versus* wild type Mb is observed for the F43H/H64L mutant. The Vmax values for one-electron oxidations by the Mbs are well correlated to the varied reactivities with H_2O_2. The functions of the distal histidine as a general acid-base catalyst are examined based on the reactions with cumene hydroperoxide and cyanide, and only the histidine in F43H/H64L Mb is suggested to facilitate the heterolysis of peroxide bond. The X-ray crystal structures of the mutants confirm that the distal histidines in F43H/H64L Mb and peroxidase are similar in distance from the heme iron while the distal histidine in L29H/H64L Mb is located too far to enhance the heterolysis (Figure 1). Our results indicate that the proper positioning of the distal histidine is essential for the activation of H_2O_2 by heme enzymes.

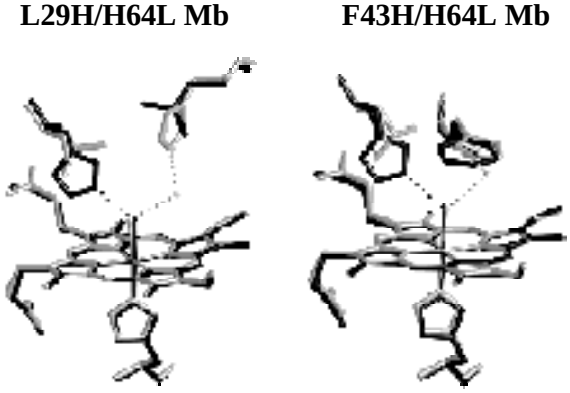

Figure 1. Crystal structures of L29H/H64L (left, gray) and F43H/H64L (right, gray) Mb mutants superimposed by wild type Mb (black).

V-A-3 Mechanistic Studies of Suicidal meso-Oxidation of Novel Iron Porphyrin Complexes as Models for the Formation of α-*Meso*-Hydroxyheme by Heme Oxygenase

Tatsuya MURAKAMI *(Kyoto Univ.)*, **Yoshihito WATANABE and Isao MORISHIMA** *(Kyoto Univ.)*

For the mechanistic studies on the formation of α-*meso*-hydroxyheme catalyzed by Heme Oxygenase (HO), we have prepared a novel iron porphyrin complex, in which less hindered *p*-chlorophenyl groups are introduced to the 5- and 15-*meso*-positions and the other two meso-positions are protected by mesityl groups; Fe^{III}BMB*p*CPP (**1a**) [BMB*p*CPP: 5,15-bis(mesityl)-10,20-bis(*p*-chlorophenyl)porphyrin]. The reaction of **1a**-trifluoroacetate (Tfa) and a small excess of *p*-nitroperbenzoic acid (*p*NPBA) has been carried out in dichloromethane containing 4 equiv of trifluoroacetic acid at -70°C. The oxidation product (2a) shows two intense absorption bands in a near-IR region and g values (6.18, 5.68, and 1.98) typical of iron(III) rhombic high spin complexes. In NMR measurements, four-splitting resonances assignable to β-pyrrole H of **2a** suggest the ring structure of C_s symmetry. These spectroscopic features readily lead us to identify **2a** as a ferric isoporphyrin complex. Further, IR and electrospray ionization (ESI) mass spectral measurements indicate **2a** bearing a *p*-nitrobenzoyloxy group at a *meso*-position. On the basis of the kinetic profile of the reaction between **1a**-Tfa and *p*NPBA, the reaction has been concluded to proceed via the formation of a *p*-nitroperbenzoate-iron(III) complex followed by an O-O bond cleavage, and more importantly, an intermediate (**3a**) prior to **2a** formation has been observed. Substituent effect of perbenzoic acid on the rate of the O-O bond cleavage shows that electron-withdrawing substituents accelerate the reaction, indicative of heterolysis of the O-O bond. When the reaction of **1a** and ^{18}O labeled *m*CPBA (Ar-C(=^{16}O)-$^{18}O_2H$) is carried out, *m*-chlorobenzoate is attached to a *meso*-position as Ar-C(=^{16}O)^{18}O-. These results demonstrate that the iron(III) isoporphyrin complex (**2a**) is formed via a *p*NPBA-iron(III) porphyrin complex and the following intermediate (**3a**) by the heterolytic O-O bond cleavage coupled with a intramolecular migration of *p*-nitrobenzoyloxy group to the *meso*-position.

V-A-4 Characterization of Polyethylene Glycolated Horseradish Peroxidase in Organic Solvents: Generation and Stabilization of Transient Catalytic Intermediates at Low Temperature

Shin-ichi OZAKI, Yuji INADA *(Toin Univ. Yokohama)* **and Yoshihito WATANABE**

[*J. Am. Chem. Soc.* **120**, 8020 (1998)]

Polyethylene glycolated horseradish peroxidase (PEG-HRP) can catalyze one- and two-electron oxidation reactions in organic solvents as well as in aqueous buffer. Even though the oxidation of guaiacol in benzene and chlorobenzene is five order of magnitude slower than in phosphate buffer, compound I and II are also involved in the catalytic cycle in organic media. Factor analysis and global fittings of rapid scan data set reveal that the formation of compound I of PEG-HRP in organic media consists of two steps: the first fast and the second slow process, and suggest the involvement of a H_2O_2-HRP complex in the catalytic cycle. The labile precursor of compound I is stabilized when PEG-HRP reacts with hydrogen peroxide in chlorobenzene at -20°C. The absorption spectrum of the precursor does not exhibit the features of hyperporphyrin spectrum but has a normal Soret as previously observed in R38L HRP. More importantly, compound I of PEG-HRP can be maintained for more than an hour at -20°C in chlorobenzene.

V-B Molecular Mechanisms of Substrate Metabolism by Heme Enzymes

Heme enzymes oxidize a variety of substrates, however, the detailed molecular mechanisms for many types of reactions including *N*-demethylation of amines, heme oxygenation, etc, are still obscure. Our efforts have been concentrated on the elucidation of the *N*-demethylation and heme oxygenation.

V-B-1 The Mechanisms of *N*-Demethylation Catalyzed by Heme Enzymes: Direct Observation of *N*-Demethylation by Compound I of Horseradish Peroxidase and Its Model Complex

Yoshio GOTO, Yoshihito WATANABE, Shunichi FUKUZUMI *(Osaka Univ)*, **Jeffry P. JONES** *(Univ. Rochester)* **and Joseph P. DINNOCENZO** *(Univ. Rochester)*

[*J. Am. Chem. Soc.* in press]

To elucidate the mechanisms of *N*-demethylation catalyzed by heme enzymes, we have employed two direct observation systems i.e., the *N*-demethylation of *p*-substituted *N*,*N*-dimethylaniline (DMA) both by horseradish peroxidase (HRP) compound I and by TMPFe(IV)=O cation radical, and evaluated the kinetic profiles. In HRP system, stepwise reduction of compound I to ferric state via compound II was observed. Linear correlation of the rate constants of each step with the oxidation potential of DMAs and no observation of kinetic isotope effect are consistent with the sequential one electron oxidation mechanism of the enzyme. On the other hand, O=$Fe^{IV}TMP^{+\bullet}$ showed isosbestic UV- spectral change to Fe^{III}TMP for the reaction with DMAs at 223K and rate constants are

linearly dependent on the oxidation potential of DMAs. Thus the demethylation by $O=Fe^{IV}TMP^{\bullet+}$ also proceeds via electron transfer. **The observed *kinetic* and *product* deuterium isotope effect profiles indicate that the electron transfer is followed by hydrogen atom transfer from $DMAs^{\bullet+}$ to $O=Fe^{IV}TMP$ in competition with the back electron transfer** (Scheme 1)**.**

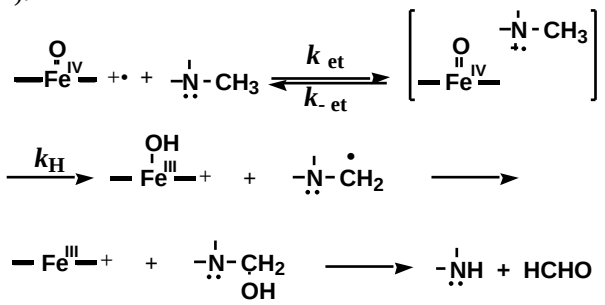

Scheme 1. *N*-Demethylation of amines by O=Fe(IV) porphyrin π-cation radical.

V-B-2 Effects of the Arrangement of a Distal Catalytic Residue on Regioselectivity and Reactivity in the Coupled Oxidation of Sperm Whale Myoglobin Mutants

Tatsuya MURAKAMI *(Kyoto Univ.)*, **Isao MORISHIMA** *(Kyoto Univ.)*, **Toshitaka MATSUI, Shin-ichi OZAKI, Isao HARA, Hui-Jun YANG and Yoshihito WATANABE**

The coupled oxidations of sperm whale myoglobin (Mb) mutants (Figure 1) are performed to examine active site residues controlling the regiospecific heme degradation. HPLC analysis of biliverdin isomers shows that L29H/H64L Mb almost exclusively gives biliverdin IXγ although H64L and wild type Mb mainly affords the α-isomer. Relocation of the distal histidine at the 43, and 107 position increases the amount of γ-isomer to 44 and 22%, respectively. Interestingly, the increase in the ratio of γ-isomer is also observed by a single replacement of either His-64 with Asp or Phe-43 with Trp. It appears that the polarity of the active site as well as hydrogen bonding between oxygen molecule bound to the heme iron and His or Trp is important in controlling the regioselectivity. The results of coupled oxidation kinetics, autooxidation kinetics, and redox potential of Fe^{3+}/Fe^{2+} couple are discussed with regards to their implications for the active site and mechanism of heme oxygenase.

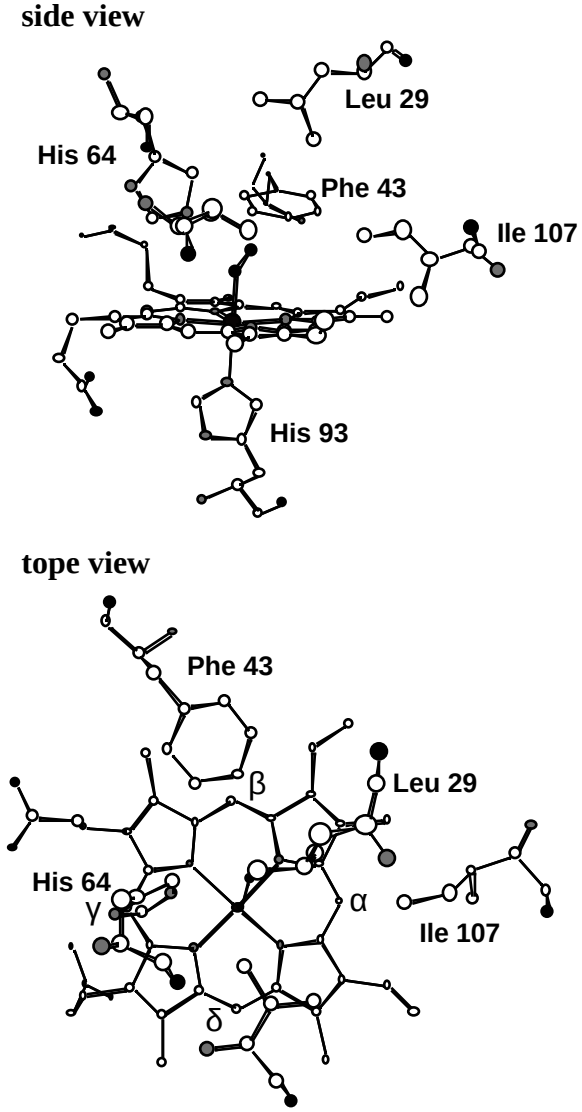

Figure 1. Top and side views of an oxy-form of the myoglobin active site.

V-C Model Studies of Non-heme Proteins

Non-heme proteins play important roles in biological redox processes. Many reactions catalyzed by the non-heme enzymes are quite similar to those by hemoproteins. We are interested in the active intermediates responsible for oxidation and oxygenation by non-heme enzyme, especially the similarity and differences.

V-C-1 A Model Complex for an Active Form of Soybean Lipoxygenase-1

Seiji OGO, Senji WADA, Masakazu IWASE *(Nagoya Inst. Tech.)*, **Akira WADA** *(Nagoya Inst. Tech.)*, **Manabu HARATA** *(Nagoya Inst. Tech.)*, **Koichiro JITSUKAWA** *(Nagoya Inst. Tech.)*, **Hideki MASUDA** *(Nagoya Inst. Tech.)*, **Hisahiko EINAGA** *(Nagoya Inst. Tech.)* **and Yoshihito WATANABE**

[*Angew. Chem. Int. Ed. Engl.* **37**, 2102 (1998)]

Lipoxygenases (LOs) are mononuclear non-heme iron enzymes which catalyze the peroxidation of polyunsaturated fatty acids and fatty acid esters containing the *cis,cis*-1,4-diene moiety to the corresponding 1-hydroperoxy-*trans,cis*-2,4-diene. We have studied synthesis, structure, and spectroscopic properties of a 6-coordinate (hydroxo)iron(III) complex

[Fe(TNPA)(OH)(PhCOO)]ClO_4 (**1**, TNPA = tris-(6-neopentylamino-2-pyridylmethyl)amine) which is the first structural model for the active center of ferric SLO-1 with a hydroxo ligand. Complex **1** has been characterized by X-ray structure analysis (Figure 1), UV/Vis, IR, EPR, and electrospray ionization mass spectrometry (ESI-MS). Complex **1** has cis-configuration between the OH^- ligand and the PhCOO- or three NH ligands of TNPA. The proposed core structure of ferric SLO-1 also has *cis*-configuration between the hydroxo ligand and the carboxylato ligand of C-terminal isoleucine or carboxamidato ligand of asparagine. The *cis*-configurations appear to be important for the formation of intramolecular hydrogen bonds which stabilize the (hydroxo)iron core structure of ferric SLO-1.

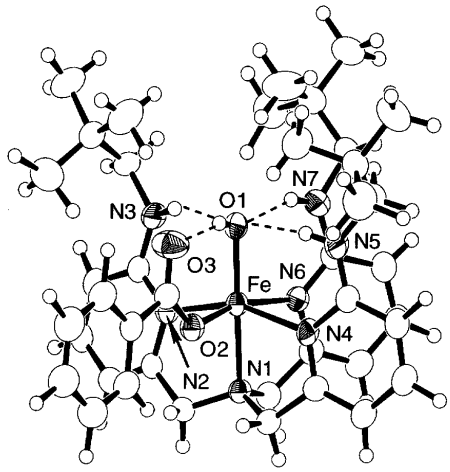

Figure 1. ORTEP drawing of [Fe(TNPA)(OH)(PhCOO)]-ClO_4 (**1**).

V-C-2 Functional Model Chemistry for Manganese(II)-Dependent Catechol Dioxygenases

Takuzo FUNABIKI *(Kyoto Univ.)*, **Tomoyuki ITO** *(Kyoto Univ.)*, **Hajime MATSUI** *(Kyoto Univ.)*, **Atsushi FUKUI** *(Kyoto Univ.)*, **Satohiro YOSHIDA** *(Kyoto Univ.)*, **Seiji OGO and Yoshihito WATANABE**

Catechol dioxygenases play key roles in the metabolism of various aromatic compounds, converting aromatics to aliphatics with insertion of molecular oxygen between a C-C bond of a benzene ring. It is well known that this reaction is catalyzed by nonheme iron oxygenases: Fe^{3+} enzymes catalyze mainly the intradiol oxygenation by a C1-C2 bond fission, and Fe^{2+} enzymes catalyze the extradiol oxygenation by a C2-C3 or C1-C6 bond fission. Besides the iron enzymes a manganese-dependent catechol dioxygenase is known to catalyze the extradiol cleavage. The similarity of the coordination environment to the iron(II) enzymes has been suggested, but little has been studied about its reactivity from both sides of enzymatic and model studies. An example reported is the oxygenation by a penicillamine-manganese complex(II), but no product analysis has been performed to confirm the extradiol oxygenation. As the first step for the functional model study for manganese-dependent catechol dioxygenases, we here first report the intradiol cleavage by a nonheme manganese complex via a semiquinonatomanganese(II) species. The present results give the support for the radical intermediate species in the oxygenation of catechols proposed for iron enzymes. In the iron system, the semiquinonate radical character caused by an electron transfer from the ligand to iron(III) has been suggested by the NMR and UV/VS spectroscopic data, but the radical species has not been detected. We here report EPR and UV/VS evidences for that species which reacts with oxygen.

V-D Transition Metal Oxide Clusters

Organometallic oxide clusters with cubic and incomplete cubic frameworks have useful applications as homogeneous and heterogeneous catalysts for reactions such as the oxidation and metathesis of propene. Understanding of the formation mechanisms of such oxide clusters may lead to the further development of synthetic methodologies for the construction of desired clusters having efficient catalytic ability for hydrocarbon transformations.

V-D-1 Direct Observation by Electrospray Ionization Mass Spectrometry of a Key Transient Intermediate in the Formation of a Double Bookshelf-Type Oxide Cluster

Satoshi TAKARA *(Osaka City Univ.)*, **Seiji OGO, Takanori NISHIOKA** *(Osaka City Univ.)*, **Isamu KINOSHITA** *(Osaka City Univ.)*, **Kiyoshi ISOBE** *(Osaka City Univ.)* **and Yoshihito WATANABE**

An organometallic oxide cluster $[(n\text{Bu})_4\text{N}]_2[(\text{Cp*-Rh}^{\text{III}})_2\text{Mo}^{\text{VI}}_6\text{O}_{20}(\text{OMe})_2]$ (**1**) with a multi-incomplete cubic framework was obtained from the reaction of $[\{\text{Cp*Rh}(\mu\text{-Cl})\text{Cl}\}_2]$ and $[(n\text{Bu})_4\text{N}]_2[\text{Mo}_2\text{O}_7]$ in MeOH. We have investigated the formation mechanism of **1**, by electrospray ionization mass spectrometry (ESI-MS) which is a powerful tool used in identification and characterization of unstable intermediates generated in solution. A transient intermediate, $[\text{Cp*RhMo}_3\text{O}_8\text{-(OMe)}_5]^-$ (**P_{im}**) in the formation of cluster **1** in MeOH at -78˚C was observed by ESI-MS. In order to gain further insight into the mechanism of the formation of **P_{im}**, time-dependent and deuterium-labeling experiments using $[(\text{Cp*-d6})\text{RhCl}_2]_2$ and CD_3OD have also been carried out. ESI-MS results established that the labeled Cp*-d6 and methoxo (OCD_3) ligands are incorporated into **P_{im}**.

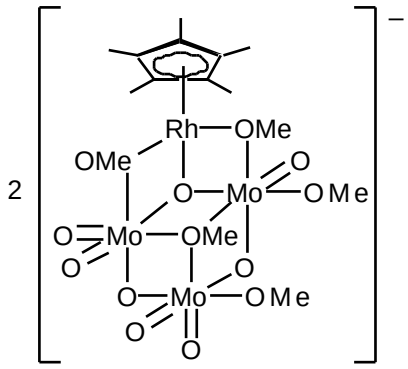

(**P$_{im}$**)

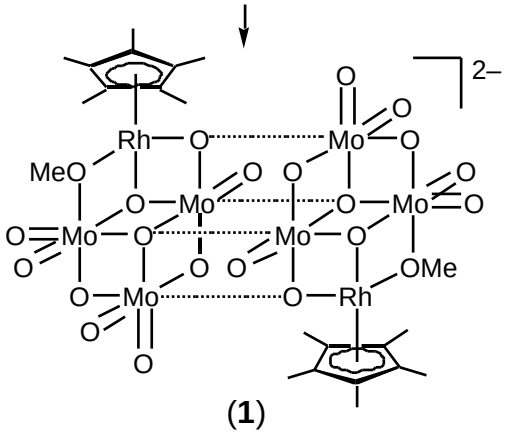

(**1**)

V-E Aqueous Organometallic Chemistry

Aqueous organometallic chemistry is a relatively new and exciting area that has primarily focused on the reactions of organometallic compounds with water soluble substrates in aqueous solution. We have studied chemo- and diastereoselective reactions of organometallic complexes as catalyst precursors in aqueous solution.

V-E-1 Synthesis and Structure of a New Water Soluble Rhodium(III) Complex

Nobuyuki MAKIHARA, Seiji OGO and Yoshihito WATANABE

Refluxing $RhCl_3 \cdot {}_3(H_2O)$ with 2-(tetramethylcyclopentadienyl)-4-methylphenol (Cp^t–H_2)[1)] in methanol generates the organometallic complex $[(Cp^t–H)Rh^{III}Cl_2]_2$ (**1**); the crystal structure of **1** was determined by X-ray analysis. Complex **1** reacts with $AgBF_4$ in water at ambient temperature to form the water soluble organometallic complex $[(Cp^t)Rh^{III}(OH_2)_2]\cdot(BF_4)$ (**2**). ^{1}H-NMR and electrospray ionization mass spectrometry (ESI-MS) have shown that complex **2** has two perpendicular (Cp^t and 4-methylphenolato) planes as the result of the formation of Rh–O(4-methylphenolato) bond. Applications of complex **2** as a catalyst precursor for selective oxidations and reductions of water soluble substrates in aqueous solution are currently under investigation.

Reference

1)Y. Chen, P. Fu, C. L. Stern and T. J. Marks, *Organometallics* **16**, 5958 (1997).

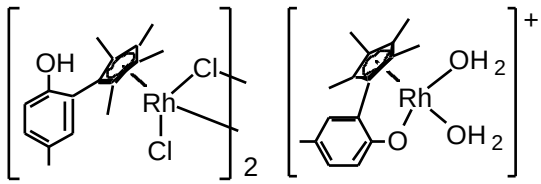

(**1**) (**2**)

V-F Construction of New Molecule-Based Magnets

Construction of molecular based magnetic materials which have well-defined one- or two-dimensional magnetic structure is a scientific subject of increasing interest. Heterospin systems consisting of paramagnetic transition metal

ions and organic free radicals as ligands constitute one of the mainstreams of such studies. Several of these materials have been established to have finite critical temperature of a ferro- or ferrimagnetic transition.

We have introduced a new strategy of employing π-conjugated polyaminoxyls as ligands in which the 2*p*-spins of the NO groups interact ferromagnetically ($J_1 > 0$). The dimensionality of the complex and the sign and magnitude of the exchange coupling between the neighboring spins may be readily tuned by this strategy. Depending on the nature of the additional interchain or interlayer interaction, the polymers are expected to become an antiferromagnet or ferri/ferromagnet. By modifying and extending this design strategy to bis- and tris(aminoxyl) radicals having triplet and quartet ground states, respectively, we have been able to construct with the aid of magnetic metal ions one-dimensional (1D) chain, two-dimensional (2D) network and three-dimensional (3D) parallel-crosses structures in which both the organic 2p and metallic 3d spins have been ordered in macroscopic scales. Since such a rational approach by self-assembly to the tailored extended systems having relevant physical properties is of great importance in materials synthesis.

V-F-1 Tacticity vs. Dimension of the Extended Structures in the Crystals of Heterospin Magnets Made of Transition Metal Complexes with Poly(aminoxyl) Radical

Hiizu IWAMURA *(Kyushu Univ.)*, **Katsuya INOUE and Noboru KOGA** *(Kyushu Univ.)*

[*New J. Chem.* **22**, 201 (1998)]

Bis- and tris(aminoxyl) radicals form with $M(hfac)_2$ {M = Mn(II) or Cu(II), and hfac = hexafluoroacetyl-acetonate} crystalline complexes having extended structures. Organic 2p and metal 3d spins in the complexes order at 3.4-46 K depending on the dimensions of the extended structures and the magnitude of exchange coupling between the adjacent spins. We have studied the crystal structures more carefully in a systematic manner to find that dimensionality of the crystal structures in these heterospin magnets is closely related to tacticity of the polymeric structures. The results obtained hereby will be of use in establishing a design strategy for tailored 3-D magnetic structures with high transition temperature on the basis of magnetic metal ions and high-spin organic polyradicals. In the crystals of one-dimensional systems, the polymeric chains are isotactic in that free radical have the same sign of chirality along any given chain (Figure 1). The polymeric chains are syndiotactic and crosslink to form two-dimensional honeycomb (Figure 2) or three-dimensional parallel-crosses networks (Figure 3).

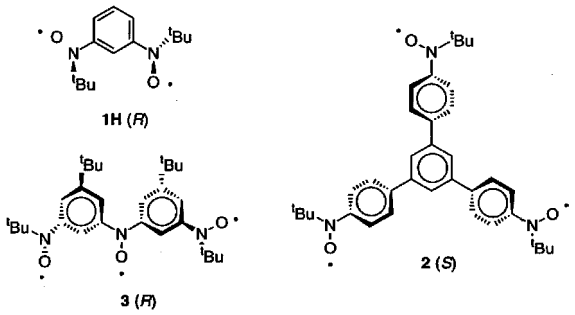

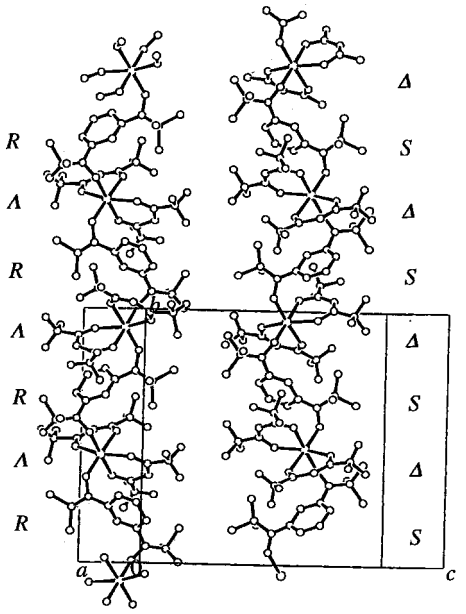

Figure 1. The one dimensional chains of $[Mn^{II}(hfac)_2 \cdot \mathbf{1H}]$ extending along the b axis.

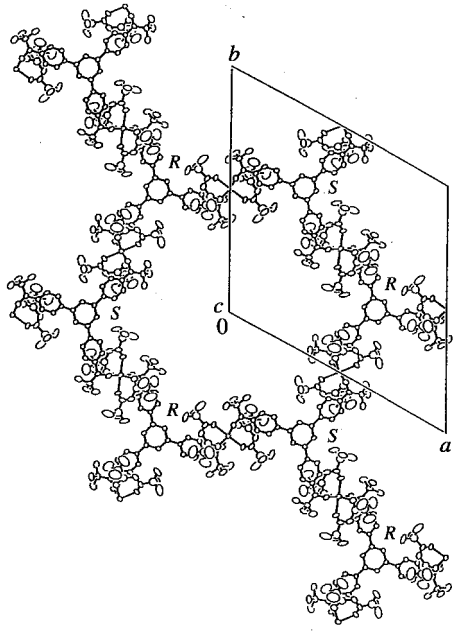

Figure 2. The complex $[\{Mn^{II}(hfac)_2\}_3 \cdot \mathbf{2}_2 \cdot n\text{-}C_7H_{16}]$ viewed down the c axis, showing the formation of two dimensional hexagonal nets. The n-C_7H_{16} molecules are disordered and not shown.

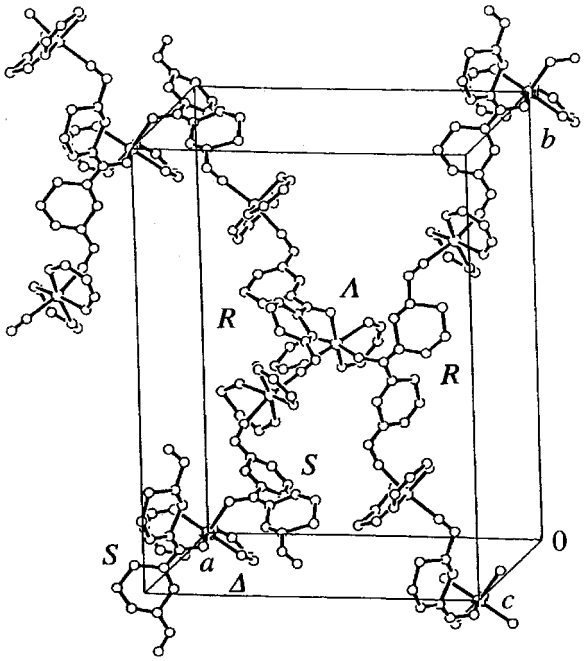

Figure 3. Three dimensonal crossed parallel structure of $[\{Mn^{II}(hfac)_2\}_3 \cdot \mathbf{3}_2]$. The CF_3 and $(CH_3)_3C$ groups are not shown for clarity.

V-F-2 Study of Magnetization and Magnetic Anisotropy of the Organometallic Complex between the Trinitroxide Radical and Bis(Hexafluoroacetylacetonato)Manganese(II)

Ashot S. MARKOSYAN, Takashi HAYAMIZU *(Kyushu Univ.)*, **Hiizu IWAMURA** *(Kyushu Univ.)* **and Katsuya INOUE**

[*J. Phys., Condens. Matter* **10**, 2323 (1998)]

A single crystal of the metal-radical complex $\{Mn(hfac)_2\}_3(\mathbf{3})_2$, where (**3**) is a trisaminoxyl radical (See previous part) with a quartet ground state, was grown. The magnetization was measured along the principal crystallographic axes in the range 1.8-300K. The compound was found to order ferrimagnetically at T_C = 45 ± 1K with collinear antiparallel alignment of the Mn- and (**3**)-magnetic spins along the c-direction. The paramagnetic susceptibility was treated in the quantum-classical approximation by taking into account the weak positive exchange interaction between the Mn(2) ions and one-dimensional ferrimagnetic ···-Mn(*1*)-(3)-Mn(*1*)-··· chains, in which trimer molecules composed of one Mn(*1*) and two 1/2 spins of different triradicals can be isolated (Figure 1). The anisotropy constants were evaluated and the anisotropy energy was estimated. Anisotropy of the paramagnetic susceptibility, which can be detected up to 55 K, was observed (Figure 2). The anisotropic effects are attributed both to the single-ion splitting of the Mn energy levels and the dipole-dipole interaction between the magnetic spins.

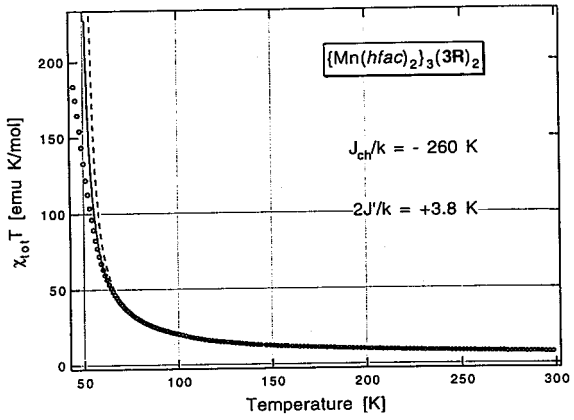

Figure 1. The temperature dependence of the product χ T of the $\{Mn(hfac)_2\}_3(\mathbf{3})_2$ complex in the paramagnetic temperature range. Open circles show the experimental data; the solid and dashed lines were calculated for the fixed trimer spin $S = 2/3$ in the quantum-classical and classical-classical approximations, respectively.

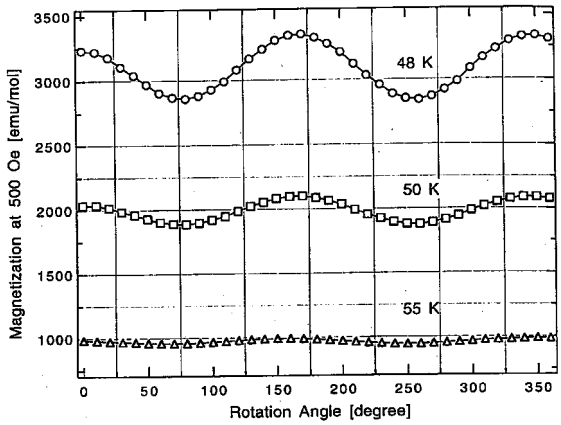

Figure 2. The angilar dependence of the low-field magnetization of the complex at different temperatures in the paramagnetic region measured in the (*ac*) crystallographic plane.

V-F-3 Magnetic Properties of Polymeric Chain Complex Made by 5-Bromo-1,3-Bis(*N-tert*-butyl-*N*-oxy-amino)benzene and Cu(II)(hfac)$_2$

Katsuya INOUE, Fumiyasu IWAHORI and Hiizu IWAMURA *(Kyushu Univ.)*

Bis(hexafluoroacetylacetonato)copper(II), $Cu(hfac)_2$, reacts with the triplet bisaminoxyl radical 5-bromo-1,3-bis(*N-tert*-butylaminoxyl) benzene **1**, to yield a distorted square-pyramidal adduct of formula $\mathbf{1}_2 \cdot [Cu(hfac)_2]_3$. The X-ray crystal structure shows that it crystallizes in the space group *P*1, with a = 12.469(2) Å, b = 15.278(2) Å, c = 11.602(2) Å, a = 104.59(1)°, b = 111.86(1)°, g = 88.32(1)°, and Z = 1. The complex makes 1-dimensional polymeric (···M-**1**-M-M-**1**-M-**1**-M-M-**1**···, M = Cu $(hfac)_2$) chain. (Scheme I) The magnetic data shows that a structural transition at ca. 48K. The structural transition shows temperature hystereisis (Figure 1). From the structural and magnetic analysis, the 1-D chain consisting of three different interaction ferro- (J_1, $J_2 > 0$) and antiferromagnetic ($J_3 \ll 0$) couplings has been realized. The exchange interaction value of 30.3 K ($2J/k_B$ value) between Cu_A

and NO group was estimated by linear three spin analysis. A structural transition occurred at ca. 48 K, the transition was assumed that the one of ferromagnetic interactions between three linear spins (NO—Cu_A—NO) changes to antiferomagnetic. (Scheme Ib)

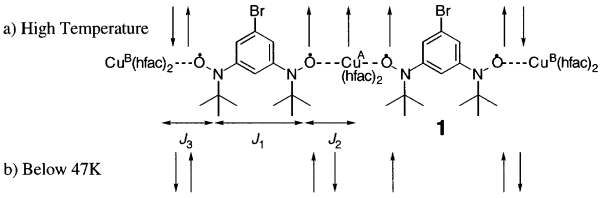

Scheme 1.

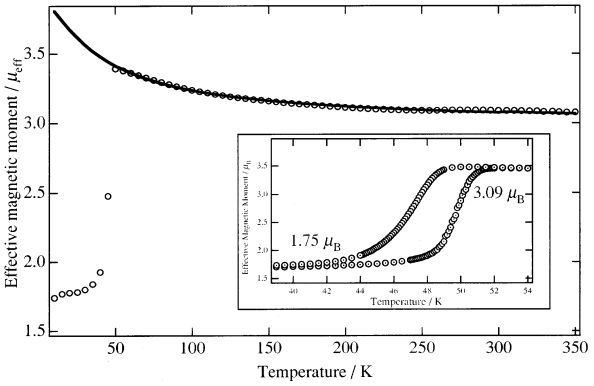

Figure 1. Observed magnetic moment versus *T* plots for the complex $\mathbf{1}_2 \cdot [Cu(hfac)_2]_3$ measured at a magnetic field of 50000 Oe. The inset shows the m_{eff} versus *T* plots of 40-55 K region. Solid lines are calculated with the linear trimer model (50-300 K).

V-G Synthesis of Chiral Molecule-Based Magnets

There is a phenomenological resemblance between natural and magnetic optical activity. The former is due to the handedness of molecular structure, whereas the latter is due to the magnetic field-induced circular dichroism. In 1984 Barron and Vrbancich call "magneto-chiral dichroism" (MChD) for a link between two phenomena. In 1997, Rikken and Raupach observed the MChD effect of tris(3-trifluoroacetyl-±-camphorato)europium (III) in the paramagnetic state. However, the MChD effect in the paramagnetic state is small. It's important to make the fully chiral molecule-based magnets, which expected to be strong MChD effect. There are still no examples of molecule-based chiral magnet. Novel properties are expected for such compounds.

The design of molecular materials with interesting electrical and/or magnetic properties is one of the major challenges of science in the last few years. It's possible to modify the molecular structure in the molecule-based magnetic materials. Recently, we introduced a strategy of using π-conjugated polyaminoxyl radicals with high-spin ground states as bridging ligands for magnetic metal ions in order to assemble and align the electron spins on a macroscopic scale. The crystal structures of these complexes are known, and some cases, the magnetic structures are analyzed. The dimensionality of the complex and the sign and magnitude of the exchange coupling between the neighboring spins may be readily tuned by this strategy. When we use a bidendate bisaminoxyl radicals as ligand and manganese(II) hexafluoroacetylacetonate, $Mn(II)(hfac)_2$, we can make one-dimensional complexes. If we use chiral triplet bisaminoxyl radicals for the construction of one-dimensional magnet, we can expect to make chiral molecule-based magnets.

V-G-1 Synthesis and Magnetic Properties of Chiral Organic Triplet Bisaminoxyl Radical

Hitoshi KUMAGAI and Katsuya INOUE

It is important to synthesize chiral magnetic compounds having ligating sites for construct chiral magnets. Nevertheless, only one example of pure organic chiral radical was reported. Novel properties are expected for such compounds. 1,3-substituted bisaminoxyl benzene biradical has been established to have a triplet ground state with a large intramolecular ferromagnetic interaction (J_1/k_B > 300 K) and has ligating capabilities. Here we report for the synthesis and characterization of a triplet organic diradical having not only a chiral carbon center but also ligating sites. A chiral triplet organic diradical 1,3-bis(*N-tert*-butyl-amino-*N*-oxyl)-5-{1-methyl-1-((*S*)-2-methylbutoxy)-ethyl}benzene (1) was synthesized and characterized. The temperature dependence of magnetic susceptibility was analyzed by a Bleany-Bowers type singlet-triplet model. (Figure 1) This result indicates that the two aminoxyl radical centers which are coupled ferro-magnetically within the organic radical molecule ($-2J/k_B$ = 461.8 K).

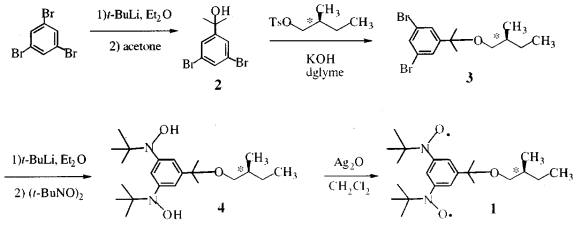

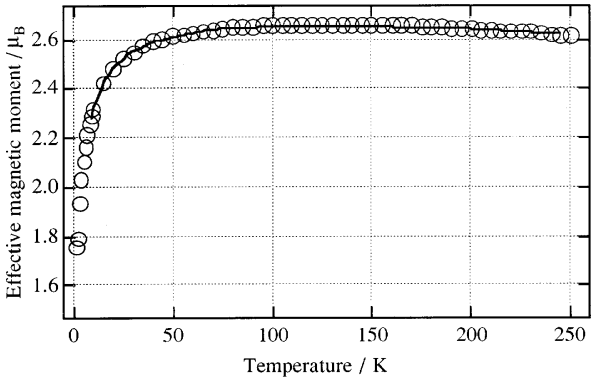

Figure 1. Observed effective magnetic moment vs. T plot for the diradical **1** measured in a magnetic field of 5000 Oe. Solid line is calculated by a Bleany-Bowers type model for the diradical **1**.

V-G-2 A Chiral Molecule-Based Metamagnet Made by Chiral Triplet Organic Radical and Manganese Ion

Hitoshi KUMAGAI and Katsuya INOUE

When we use a chiral bisaminoxyl radical for the ligand, a chiral one-dimensional structure was expected. Brown crystals of $\{\mathbf{1}\cdot Mn(II)(hfac)_2\}_n$ were obtained by mixing the 1,3-Bis (*N-oxy-tert*-butylamino)-5-{(S)-2'-methylbutyloxy}-*iso*-propylbenzene (**1**) and bis(hexafluoroacetylacetonato)manganese(II) $\{Mn(II)\cdot(hfac)_2\}$ in diethyl ether/*n*-heptane. A single crystal is triclinic, space group *P*1 (No. 1), with a = 11.0001 Å, b = 11.8204 Å, c = 17.7155 Å, α = 81.6093°, β = 84.8131°, γ = 63.5208°, V = 2038.9523 Å^3, and D_X = 1.380 g/cm^3 for Z = 1. An X-ray crystal structure analysis revealed the formation of a DNA strand type (*R*)-helical one-dimensional polymeric structure. It not only contains a (*S*) chiral carbon center but also (*R*) *C2* chiral skeleton of the organic ligand (Figure1). Each of the two aminoxyl radical centers which are mutually coupled ferromagnetically within the organic radical molecule is coupled antiferromagnetically to the d^5 manganese(II) ions. The temperature dependence of the magnetization revealed that the heterospin system behaves as a metamagnet below 5.4 K (Figure 2).

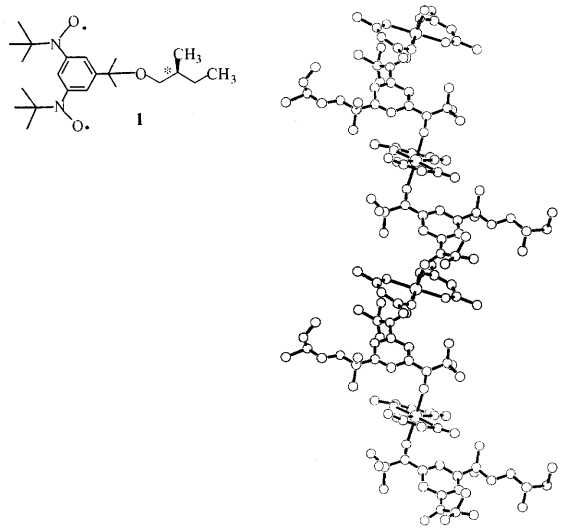

Figure 1. The X-ray crystal structure of the complex of $[\mathbf{1}\cdot Mn(II)(hfac)_2]_n$. Hydogen atoms are omitted for clarity. View along the *b* axis.

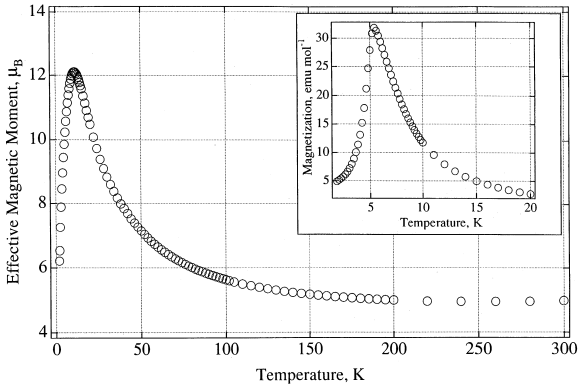

Figure 2. Temperature dependence of magnetic moment in a field of 5000 Oe of a polycrystalline sample of $[\mathbf{1}\cdot Mn(II)(hfac)_2]_n$. Inset shows the temperature dependence of magnetization at a field of 5 Oe of a polycrystalline sample.

V-H Synthesis and Characterization of Light Induced Spin-Crossover Complexes

The first transition metal compounds with d^4, d^5, d^6 and d^7 electron configuration are usually classified into two categories, i.e. high-spin and low-spin compounds depending on the strength of ligand field. However, there are compounds of which the ligand field strength is comparable to a spin-pairing energy, these complexes exhibit a temperature dependent spin-transition and this phenomenon is called spin-crossover. Spin-crossover complexes exhibit a temperature or pressure dependent spin transition. The spin-atate transition takes place through the thermal population of the high-spin and low-spin levels. A quantitative light-induced $^1A_1$(low-spin) $\rightarrow$ $^5T_2$(high-spin) transformation has been achieved in a number of iron(II) spin-crossover complexes in solid state, at a temperature much lower than that of the thermal transition (« 40 K), by irradiation the sample into the spin-allowed d-d or MLCT absorption bands of the stable low-spin species. The metastable high-spin state which forms in these conditions can remain trapped, with a practically infinite lifetime. This phenomenon is explained on the basis of light-induced excited spin state trapping; LIESST. We report the spin-state transition of the iron(III) complexes occurs by a new strategy which consists in varying ligand field strength under photochemical cis-trans isomerization of ligands, of which phenommenon has been able to be observed by using azobis(4-pyridine) analogs at relatively high temperature.

V-H-1 Synthesis and Magnetic Properties of Binuclear Iron(III) Complex Containing Photoisomerization Ligand

Shinya HAYAMI, Katsuya INOUE and Yonezo MAEDA *(Kyushu Univ.)*

[*Chem. Lett.* in press]

Binuclear iron(III) spin-crossover complexes with salten and az ligands $[Fe_2(salten)_2(az)](BPh_4)_2$ (salten is 1:2 condensation products of dipropylenetriamine and salicylaldehyde, and az is azobis(4-pyridine) (Scheme 1) were synthesized. The crystal structure, Mössbauer spectra, magnetic susceptibilities, electronoc spectra of the complex were examined. The X-ray structure of the complex were determined (Figure 1). Crystal data for the complex: $Fe_2O_4N_{10}C_{98}B_2H_{94}$, space group $P2_1/c$, Z = 2, a = 16.422(7), b = 16.005(6), c = 16.565(8) Å, β = 108.47(3)°, V = 4129(2) Å^3, R = 0.075, R_w = 0.060, 8608 reflections. The complex exhibited spin-crossover behavior depending on temperature, interexchange the rates of which are rapid compared to the Mössbauer time scale (10^7/s). The electronic spectra of the complex with photoisomerization ligamd (az) shifted reversibly by light irradiation in solution and irreversibly in solid state on the LMCT bands (Figure 2).

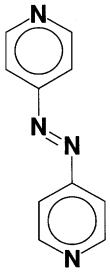

Scheme 1. Structure of az.

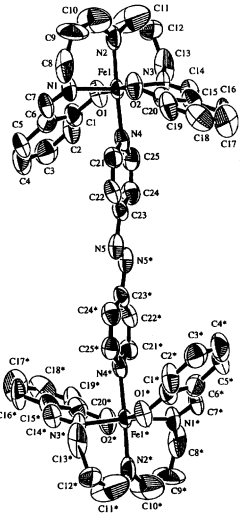

Figure 1. ORTEP view of the cation for $[Fe_2(salten)_2(az)](BPh_4)_2$. All hydrogen atoms are ommited for clarity.

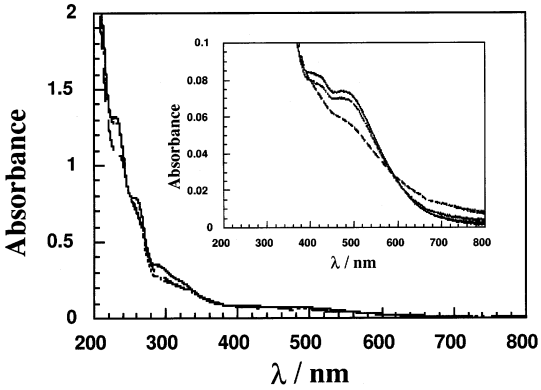

Figure 2. Absorption spectra at room temperature of $[Fe_2(salten)_2(az)](BPh_4)_2$ in acetonitrile solution before (——) and after (----) irradiation at lexc=300 nm, and 3 days after discontinuance of the irradiation (——). Insert: corresponding absorbance evolution in the LMCT band area.

V-I Synthesis and Characterization of Quantum-Spin Systems

Quantum spin systems have been much attracted for several decades. Quite different ground state is expected and the properties are open to research. In order to realize quantum spin systems, the spin-source should be isotropic. Organic radicals consisting only of light elements are regarded as ideal isotropic spin systems and are suitable for such studies. Focusing on this character, we are designing novel organic polyradicals to construct various lattice systems whose ground state is interested.

In 1983, Haldane conjectured the difference between a Heisenberg antiferromagnetic chain of integer-spin magnitude and that of half-integer-spin magnitude: Properties of integer-spin antiferromagnetic Heisenberg chain are characterized by the existence of a finite excitation gap above the unique ground state. Using organic biradicals, we can realize the intermediate spin state between spin-1/2 and spin-1. We have succeeded in tuning the intramolecular exchange couplings in organic biradicals by chemical modifications and arranging the biradicals to form low-dimensional antiferromagnetic lattices. The ground state properties are also studied in detail.

V-I-1 Ground State Properties of One- and Two-Dimensional Antiferromagnetic Heisenberg Spin Systems Made of Stable Organic Biradicals

Yuko HOSOKOSHI, Hiroki NAKANO *(ISSP Univ. Tokyo)***, Kohichi TAKIZAWA** *(ISSP Univ. Tokyo)***, Tsuneaki GOTO** *(ISSP Univ. Tokyo)***, Minoru TAKAHASHI** *(ISSP Univ. Tokyo)* **and Katsuya INOUE**

The ground state properties of antiferromagnetic

lattice systems of organic biradicals with $S = 1$ are examined. Among them, only F_2PNNNO exhibits an energy gap above the singlet ground state. The temperature dependence of the paramagnetic susceptibilities (χ_p's) of F_2PNNNO has a maximum at around 16 K and goes down to zero as temperature decreases. The magnetization isotherm of F_2PNNNO was measured at 0.5 K upto 40 T. The magnetization values below 8 T keep zero, take a constant value between 15-25 T at the half-value of the saturated magnetization and above 30 T, reach the saturated value corresponding to the parallel alignment of 2 mol of S = 1/2 species. (Figure 1). This behaviour is quite different from that of PNNNO, which shows monotonous increase of the magnetization. Both crystals of PNNNO and F_2PNNNO involve very similar chain structures, but interchain short contacts exist only in F_2PNNNO. We analyze the magnetic properties of PNNNO and F_2PNNNO based on the one-dimensional and two-dimensional model, respectively. The exchange parameter sets of $2J_F/k_B$ = 638 and $2J_{AF}/k_B$ = -14.5 K for PNNNO, and $2J_F/k_B$ = 407 and $2J_{AF}/k_B$ = -7.4, and $2J'_{AF}/k_B$ = -76 K for F_2PNNNO well reproduce the experimental results, where J_F, J_{AF}, and J'_{AF} represents the intramolecular ferromagnetic coupling, intrachain antiferromagnetic coupling, and interchain antiferromagnetic coupling, respectively. We must mention that F_2PNNNO is a quite rare example of two-dimensional system with an energy gap.

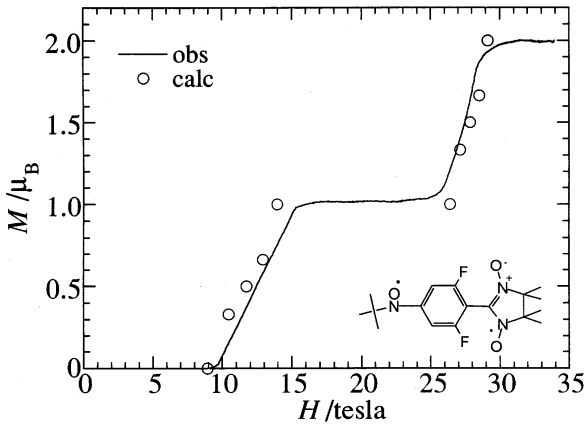

Figure 1. Magnetization process of F_2PNNNO at 0.5 K. Circles represent the calculation based on the two-dimensional model.

V-I-2 Construction of One-Dimensional Chain and Railroad-Trestle Using Organic Radicals

Yuko HOSOKOSHI, Keiichi KATOH *(Sci. Univ. Tokyo and IMS)***, Kenji MORI** *(Sci.Univ. Tokyo)* **and Katsuya INOUE**

We have synthesized organic monoradicals, F_2-PIMNH and Cl_2PIMNH to form chain structures using the hydrogen bonding between the NO and NH groups (-NO—HN-). In fact, both crystals involve such a hydrogen bonding, which yield small antiferromagnetic exchange coupling of *ca*. 3 K. Moreover, the crystals of F_2PIMNH has another hydrogen bonding as the second nearest contact to form a railroad trestle, whereas Cl_2-PIMNH form a simple uniform chain. The existence of an energy gap in F_2PIMNH is suggested from the temperature dependence of the static susceptibility measurements.

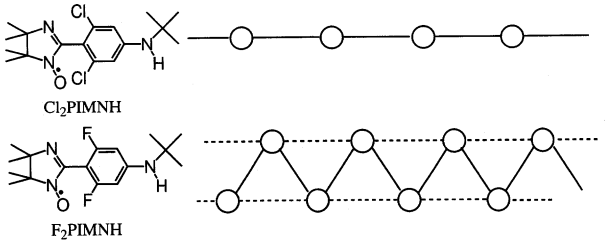

Figure 1. Schematic display of magnetic models with molecular structures.

V-J Pressure Effects on Molecular Magnetism

'Pressure' is a powerful tool to control the molecular packings and physical properties. The molecule-based materials with small densities are 'soft' and can be expected to exhibit large pressure effects. For the magnetic measurements with high-accuracy, we have developed a small high-pressure clamp cell made of Cu-Ti alloy which can be equipped to a Quantum Design SQUID magnetometer for the dc and ac magnetic measurements. The inner pressure of the clamp cell has been calibrated by the superconducting transition temperature of Pb. The maximum pressure maintained is ca. 7 kbar, the reproducibility is good, and the temperature variation of pressure in the cell is within ca 0.3 kbar.

We have already discovered that some kind of structural change can be suppressed by pressurization. We are now studying the pressure effects on the molecule-based magnetic materials in wider range. In molecular materials, the spin density are delocalized and distributed in a molecule and the spin-density-distribution plays an important role in the exchange interactions. It is attractive to control the sign of the exchange coupling by pressurization. The pressure effects on the related compounds with similar crystal structures are studied, and observed is the dimensional crossover and the change of the sign of magnetic interactions induced by pressure.

V-J-1 Pressure Effects on Organic Radicals with Ferromagnetic and Antiferromagnetic Interactions

Yuko HOSOKOSHI and Katsuya INOUE

Magnetic properties of stable organic biradicals under pressure are presented. The dimensional crossover from two-dimension to one-dimension induced by pressure is observed in F_2PNNNO, whereas the properties of the corresponding one-dimensional material, PNNNO is almost independent of the pressure. The energy gap in F_2PNNNO disappear under 3 kbar, reflecting the disappearance of the interchain interactions. (Figure 1). In the case of a quasi-one-dimensional antiferromagnet, PIMNO, the phase transition temperature become higher with applied pressure. The increase of the interchain interactions by pressurization has been observed, whereas the intrachain interactions are almost independent of the pressure.

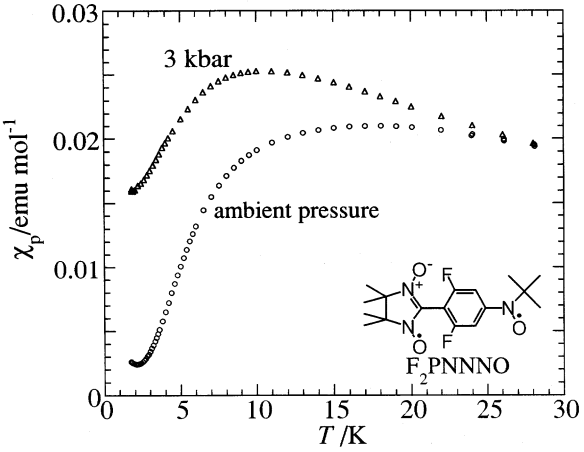

Figure 1. Temperature dependence of the paramagnetic susceptibilities of F_2PNNNO under 3 kbar compared with that at ambient pressure.

V-J-2 Pressure Effect on Mn Complexes of Bisaminoxyl Radicals

Yuko HOSOKOSHI, Kentaro SUZUKI *(Grad. Univ. Adv. Stud.)***, Katsuya INOUE and Hiizu IWAMURA** *(Kyushu Univ.)*

Organic biradical, 1,3-bis(*N*-tert-butylaminoxyl-benzene) (**1H**) makes a complex of [Mn(hfac)$_2$]·**1H** with one-dimensional chain and undergoes a metamagnetic phase transition at 5.4 K. The halogen derivatives of the biradical **1H**, replaced the hydrogen atom at 5 position by chlorine (**1Cl**) and bromine atoms (**1Br**), also form 1:1 complex with [Mn(hfac)$_2$] with one-dimensional chain and undergo ferrimagnetic phase transitions at 4.8 K and 5.3 K, respectively. The different ground states are attributed to the different sign of the interchain interactions. The slight change of the relative packing of the chain structure results in the different sign of the interchain interactions. Then, we apply pressure to these materials to change the magnitude and sign of the interchain exchange couplings.

The pressurization of the complex of [Mn(hfac)$_2$]·**1H** increases the magnitude of the antiferromagnetic interchain interactions. The transition temperature and the critical field of metamagnetic phase transition increases as increasing pressure. The critical field increases from *ca.* 200 Oe at ambient pressure to *ca.* 600 Oe under 7 kbar. The transition temperature under 7 kbar is 5.8 K.

On the other hand, the behaviour of the complex of chlorine derivative, [Mn(hfac)$_2$]·**1Cl**, under pressure is rather complicated. The temperature dependence of the ac susceptibilities under pressure shows a peak, whereas the one at ambient pressure diverges below *ca.* 4.8 K. The maximum temperature of the ac susceptibility under 4 and 7 kbar is 5.0 and 5.5 K, respectively. Moreover, the saturation rate of the magnetization at 1.8 K under pressure is slow, whereas the magnetization at 1.8 K at ambient pressure shows rapid saturation. Therefore, it is suspected that pressurization reduces the ferromagnetic distribution and induces the antiferromagnetic distribution in the interchain interactions.

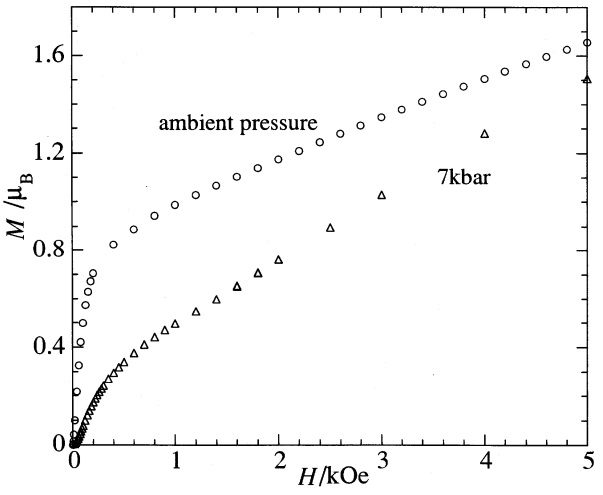

Figure 1. Magnetization isotherms at 1.8 K of [Mn(hfac)$_2$]·**1Cl**.

V-K New Charge-Transfer Complexes Exhibiting Novel Magnetic Properties

In 3d transition metals of iron, cobalt and nickel ferromagnetic state can be maintained at extremely high temperature. In contrast, a highest critical temperature (T_c) of ferromagnetic phase transition is 1.48 K in entirely s/p orbital-based organic ferromagnets, of which the first one has been discovered in a nitronylnitroxide radical crystal and successively about twenty ones have till now been prepared by using other organic radical crystals and charge-transfer (CT) complexes. In the present study we investigated the synthesis and magnetic properties of new

CT complexes with aim at achieving purely organic ferromagnets with high T_c.

V-K-1 1:2 Dimethyl-Substituted Tetracyanoquinodimethane/Its Radical Anion Mixed Salts: Ferromagnetic Behavior and High Electrical Conductivity at Room Temperature

Toyonari SUGIMOTO *(Osaka Pref. Univ. and IMS)*, **Kazumasa UEDA, Satoshi ENDO, Naoki TOYOTA, Toshiji TADA, Kei-ichiro NISHIMURA, Masakado KOHAMA, Kaoru SHIWAKU, Koji YAMAMOTO** *(Osaka Pref. Univ.)*, **Toshiyuki YAMAGUCHI, Yusaku SUENAGA and Megumu MUNAKATA** *(Kinki Univ.)*

[*Chem. Phys. Lett.* **288**, 767 (1998)]

So far, we prepared TCNQ/$TCNQ^{-\cdot}$ and $TCNQF_4$ /$TCNQF_4^{-\cdot}$ (1:2) mixed NMe_4^+ salts, which exhibited low electrical conductivities (< 10^{-2} S cm^{-1}) at room temperature. Nevertheless, for these mixed salts ferromagnetic behavior albeit in very small saturation magnetization was observed at room temperature. In order to confirm whether this anomalous magnetic behavior can also occur for the 1:2 mixed salts of the other substituted TCNQ derivatives, 1:2 mixed NMe_4^+ (**1**) and PMe_4^+ salts (**2**) of dimethyl-substituted TCNQ (DMTCNQ) with its radical anion ($DMTCNQ^{-\cdot}$) were prepared. The new 1:2 mixed salts exhibited both ferromagnetic behavior and high electrical conductivity at room temperature. The crystal structure of **2** (Figure 1) showed a composition of two different DMTCNQ /$DMTCNQ^{-\cdot}$ (1:1) and $DMTCNQ^{-\cdot}$ columns, which have significant contact with each other.

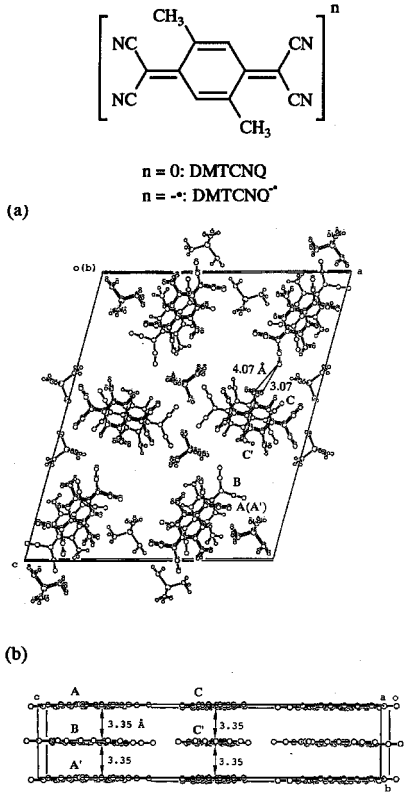

Figure 1. The crystal structure of **2**: the projections along the (a) *b* and (b) *a* axes.

V-K-2 Room-Temperature Ferromagnetic Behavior in 2,5-Diethyltetracyanoquinodimethanide Salts

Toyonari SUGIMOTO *(Osaka Pref. Univ. and IMS)*, **Kaoru SHIWAKU, Masakado KOHAMA, Kazumasa UEDA** *(Osaka Pref. Univ.)* **and Hideo FUJITA** *(Kyoto Univ.)*

Three years ago we found out room-temperature ferromagnetic behavior with small saturation magnetization for an 1:2 mixed NMe_4^+ salt of tetrafluoro-substituted TCNQ ($TCNQF_4$) with its radical anion. Subsequently, this phenomenon also was observed in 1:2 mixed Cs^+, NMe_4^+ and PMe_4^+ salts of TCNQ and dimethyl-substituted TCNQ (DMTCNQ) with their radical anions. In addition, the DMTCNQ salts exhibited high room-temperature electrical conductivities of 10-40 S cm^{-1}. Now, we investigated crystal structures, and electrical conducting and magnetic properties of NMe_4^+, PMe_4^+ and $AsMe_4^+$ salts of radical anion ($DETCNQ^{-\cdot}$) of diethyl-substituted TCNQ (DETCNQ). The crystal structure analyses showed that for the NMe_4^+ and PMe_4^+ salts one-dimensional column composed of dimerized $DETCNQ^{-\cdot}$ molecules is formed, while the two different $DETCNQ^{-\cdot}$ stacks are uniform for the $AsMe_4^+$ salt. These $DETCNQ^{-\cdot}$ salts also exhibited ferromagnetic behavior with very small saturation magnetization and coercive force, as was observed for the 1:2 mixed salts of TCNQ and DMTCNQ with their radical anions.

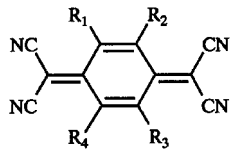

$TCNQF_4$: $R_1 = R_2 = R_3 = R_4 = F$
TCNQ: $R_1 = R_2 = R_3 = R_4 = H$
DMTCNQ: $R_1 = R_3 = Me$, $R_2 = R_4 = H$
DETCNQ: $R_1 = R_3 = Et$, $R_2 = R_4 = H$

V-K-3 Electrical Conducting and Magnetic Properties of Cesium Salts of Radical Anions of Dimethyl- and Diethyl-Substituted Tetracyanoquinodimethanes, and Tetracyanonaphthoquinodimethane

Toyonari SUGIMOTO *(Osaka Pref. Univ. and IMS)*, **Kaoru SHIWAKU, Masakado KOHAMA, Kazumasa UEDA, Satoshi ENDO, Naoki TOYOTA** *(Osaka Pref. Univ.)* **and Hideo FUJITA** *(Kyoto Univ.)*

A number of TCNQ radical anion ($TCNQ^{-\cdot}$) salts and 1:1 TCNQ/$TCNQ^{-\cdot}$ mixed salts have so far been prepared, but an 1:2 TCNQ/$TCNQ^{-\cdot}$ mixed salt is only known for the Cs^+ salt, which shows moderate room-temperature electrical conductivity on the single crystal. Furthermore, room-temperature ferromagnetic behavior with very small saturation magnetization was observed for the Cs^+ salt. The new Cs^+ salts of radical anions

(DMTCNQ$^{-\cdot}$, DETCNQ$^{-\cdot}$ and TNAP$^{-\cdot}$) of dimethyl- and diethyl-substituted TCNQ's (DMTCNQ and DETCNQ), and tetracyanonaphthoquinodimethane (TNAP) were prepared, which have molecular formulae of $Cs^+ \cdot DMTCNQ^{-\cdot}$, $\{Cs^+ \cdot DETCNQ^{-\cdot}/(Cs^+ \cdot DETCNQ^{-\cdot}) \cdot 1/2DETCNQ\}$ and $(Cs^+ \cdot TNAP^{-\cdot}) \cdot 1/2TNAP$, respectively. The $\{Cs^+ \cdot DETCNQ^{-\cdot}/(Cs^+ \cdot DETCNQ^{-\cdot}) \cdot 1/2DETCNQ\}$ and $(Cs^+ \cdot TNAP^{-\cdot}) \cdot 1/2TNAP$ salts exhibited considerably high room-temperature electrical conductivities of ca. 0.1 S cm^{-1} on the compressed pellets. The room-temperature ferromagnetic behavior was observed for the three Cs^+ salts, of which large saturation magnetization (7.3 emu mol^{-1}) was obtained for the $(Cs^+ \cdot TNAP^{-\cdot}) \cdot 1/2TNAP$ salt.

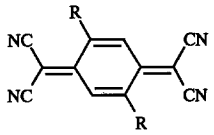

TCNQ: R = H
DMTCNQ: R = Me
DETCNQ: R = Et

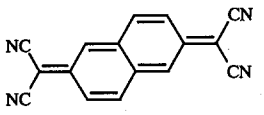

TNAP

V-K-4 Synthesis and Electrical Conducting Properties of Unsymmetrical Spiro Compounds Bearing a Tetrathiafulvalenyl Group

Masaki IWAMATSU, Kazumasa UEDA *(Osaka Pref. Univ.)*, **Toyonari SUGIMOTO** *(Osaka Pref. Univ. and IMS)* **and Hideo FUJITA** *(Kyoto Univ.)*

Single-component organic metals and furthermore superconductors are still not known, although their development is continuing to draw much attention. The first single-component organic conductor was realized in the TTF derivatives substituted with long-alkylthio or methyltelluro groups. The single-crystal electrical conducting property was semiconducting. We were rather interested in spiro compounds substituted with each of electron-donating and electron-accepting groups, which are arranged in a perpendicular manner and separated from each other, since a metallic state is expected to be increasingly stabilized by significant interaction between hole-carrying donor and electron-carrying acceptor stacks through a spiro conjugation, if the donating and accepting groups can be segregatedly stacked. As the first step, we prepared new spiro compounds (**1a** - **1d**) bearing each of dialkylthiotetrathiafulvalenyldithio and benzene- or toluene-dithio groups, and investigated their electrical conducting properties. One spiro compound, **1a** exhibited high room-temperature electrical conductivity (ca. 10^{-3} S cm^{-1}) on the compressed pellet.

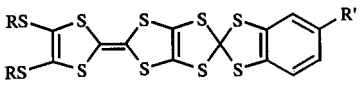

1a: R = CH_3, R' = H
1b: R = R' = CH_3
1c: R, R = -CH_2CH_2-, R' = H
1d: R, R = -CH_2CH_2, R' = CH_3

V-K-5 Synthesis, and Electrical Conducting and Magnetic Properties of Neutral Bis(tetrathiafulvalenyldithiolato) Cobalt Complexes

Kazumasa UEDA, Makoto GOTO, Yutaka KAMATA *(Osaka Pref. Univ.)*, **Toyonari SUGIMOTO** *(Osaka Pref. Univ. and IMS)*, **Satoshi ENDO, Naoki TOYOTA, Koji YAMAMOTO** *(Osaka Pref. Univ.)* **and Hideo FUJITA** *(Kyoto Univ.)*

Since the study on electrical conducting and magnetic properties of a prototype of π-d cooperative system, metallophthalocyanines, much effort has been paid for constructing various types of π-d cooperative systems and for elucidating their electrical conducting and magnetic properties. Our interest has been directed toward the synthesis of such a new type of organic complexes that an electron-donating organic ligand is bound to a magnetic metal ion through a covalent bond, and that two- or three-dimensional π conducting network is expected to be formed by π-d interaction in the crystal. Previously, we synthesized neutral bis(tetrathiafulvalenyldithiolato) copper complexes, which showed high room-temperature electrical conductivities (σ_{rt}'s) (10^{-4}-10^{0} S cm^{-1}) as result of preferential one-electron transfer from the Cu(II) atom to the TTF dithiolate radical cations. Now, the corresponding cobalt complexes (**1a-1c**) were synthesized, whose σ_{rt} values were 10^{-4}-10^{-10} S cm^{-1}. The SQUID measurement showed that the cobalt atom is in the Co(II) sate (S = 1/2). Addition of an equimolar amount of tetramethylthio-substituted TTF to **1a** brought about marked increase by ca. 10^7 in the σ_{rt} value.

V-L Desorption Induced by Electronic Transitions at the Surface of Van der Waals Condensates

The electronic excitation on the surface of a van der Waals condensate may lead the desorption of neutral and charged molecules, either in a ground state or in excited ones. The phenomena discussed here are neither thermal desorption nor direct mechanical sputtering but processes through a transformation of an electronic excitation energy into a kinetic energy of a desorbing particle. Close investigation of this DIET (Desorption Induced by Electronic Transitions) phenomena will reveal the dynamical aspect of the electronic excitation and its relaxation process at the surface. In this research project, we have revealed the desorption of the excimer, Ne_2*, and determined the absolute total desorption yield at the surface of solid Ne.

V-L-1 Exciton Induced Desorption at the Surface of Rare Gas Solids

Ichiro ARAKAWA *(Gakushuin Univ. and IMS)*

[*Mol. Cryst. Liq. Cryst.* **314**, 47 (1998)]

The nature of the exciton in rare gas solids have extensively been investigated by various experimental methods: photo-absorption, luminescence, electron energy loss spectroscopy, etc. The observation of the desorbed metastable is complementary one to the above approaches and is one of the most direct means to reveal the dynamic nature of the exciton, especially on a surface, because it detects the excited neutral species directly originated from the exciton. Many unclarified problems still remain in this field. As concerns the desorption from the S1 exciton, for example, the initial excitation and the deexcitation cascade leading to the desorption of the metastable have not been clarified yet. It is necessary to examine the fine structures in the relation between the exciton excitation and the desorption by using higher resolution spectroscopy. It has also been noticed that the phenomena are acutely sensitive to impurities adsorbed on a surface. As to some characteristic features observed in the present study, it should be clarified whether it is the nature intrinsic in a pure rare gas solid or is originated from impurities. Close investigation of the interaction with the impurities will provide a field of the study of the excitation transfer process between heteromolecules in a thick environment of condensate.

V-L-2 Desorption of Metastable Particles Induced by Electronic Excitation at the Surface of Rare Gas Solid with Hydrogen Physisorbed

Akira HAYAMA *(Gakushuin Univ.)*, **Takafumi KUNINOBU** *(Gakushuin Univ.)*, **Takato HIRAYAMA** *(Gakushuin Univ.)* **and Ichiro ARAKAWA** *(Gakushuin Univ. and IMS)*

[*J. Vac. Sci. Technol. A* **16**, 979 (1998)]

The effect of physisorption of hydrogen on the desorption of metastable particles induced by electronic excitation from the surface of rare-gas solids (Ar, Kr, and Xe) was investigated systematically. When the surface of rare-gas solid was exposed to a very small quantity of hydrogen at a temperature of about 30 K, in all cases, the desorption of hydrogen metastables was observed, and new desorption species of Kr* via cavity ejection process appeared in TOF spectra for Kr. For Ar, although no significant increase of desorption yield was found, the kinetic energy of Ar* desorbed through cavity ejection process was increased by hydrogen adsorption. These results will be discussed in terms of the change of electron affinity of the matrix and the interaction between hydrogen and rare gas molecules in excited states.

V-L-3 Desorption of an Excimer from the Surface of Solid Ne by Low Energy Electron and Photon Impact

Takato HIRAYAMA *(Gakushuin Univ.)*, **Akira HAYAMA** *(Gakushuin Univ.)*, **Takashi ADACHI** *(Gakushuin Univ.)* **and Ichiro ARAKAWA** *(Gakushuin Univ.and IMS)*

[submitted]

Desorption of an excited dimer from the surface of solid Ne initiated by a creation of an exciton was confirmed experimentally using a low energy electron and a monochromatic VUV light as excitation sources. The kinetic energy of desorbed excimer (Ne_2^* $^3\sum_u$) was found to be about (0.2±0.1) eV, which is consistent with a recent quantum mechanical calculation by Chen et al.[1] Desorption yield of the excimer in vibrationally excited states has been found to be about 10 times larger than that of vibrationally relaxed excimers. Desorption of excimers at the excitation of the first order surface exciton was found to be inefficient compared to that by the creation of bulk excitons opposed to the atomic desorption case.

Reference

1)L. F. Chen, G. Q. Huang and K. S. Song, *Nucl. Instrum. Meth. Phys. Res. B* **116**, 61 (1996).

V-M Synthesis and Physical Properties of Novel Molecular Metals

Development of organic materials which exhibit interesting electrical properties such as metallic conductivity and superconductivity has received considerable attention. A bis-fused TTF, 2,5-bis(1,3-dithiol-2-ylidene)-1,3,4,6-tetrathiapentalene (TTP) is a promising π-electron framework for preparation of stable metals down to low temperatures, because it has a ladder-like array of sulfur atoms indispensable for constructing two-dimensional network of the donors. In fact, we have found that the unsubstituted TTP has a strong tendency to afford highly conducting radical cation salts retaining metallic conductivity down to ≤ 1.2 K regardless of shape and size of counter anions. In the present study, we have developed several organic metals by means of comprehensive modification of TTP, namely i) introduction of substituents, ii) exchange of sulfur atoms in the TTP framework with selenium, iii) synthesis of TTP analogs possessing non-TTF donor unit.

V-M-1 Structural Feature of Radical Cation Salts Based on TTP and Its Selenium Analogs

Yohji MISAKI *(Kyoto Univ. and IMS)*, **Tatsuro KOCHI** *(Kyoto Univ.)*, **Masateru TANIGUCHI** *(Kyoto Univ.)*, **Tokio YAMABE** *(Kyoto Univ.)*,

Kazuyoshi TANAKA *(Kyoto Univ.)*, **Kazuo TAKIMIYA** *(Hiroshima Univ.)*, **Atsushi MORIKAMI** *(Hiroshima Univ.)*, **Tetsuo OTSUBO** *(Hiroshima Univ.)* **and Takehiko MORI** *(Tokyo Inst. Tech.)*

Two selenium analogs of TTP (2,5-bis(1,3-dithiol-2-ylidene)-1,3,4,6-tetrathiapentalene), ST-TTP and BDS-TTP have been prepared. Both donors afford many cation radical salts showing metallic conducting behavior down to liquid helium temperature. All the AsF_6 salts based on TTP, ST-TTP and BDS-TTP are isostructural to each other. The donors form conducting sheets along the *ac* plane, which are separated by insulating anion layers. The array of donors is classified as the so-called β-type (Figure 1), but the degree of dimerization in the stack is much smaller than that of β-$(BEDT\text{-}TTF)_2I_3$. It is noted that replacement of sulfur atoms with larger selenium atoms does not affect the donor array in the radical cation salts at all, whereas such a modification largely influences donor packing in the BEDT-TTF systems. For example, BETS affords κ- and λ-type salts with tetrahedral anions such as $GaCl_4^-$ and $FeCl_4^-$. In contrast, no such phase has been found in the BEDT-TTF salts with the similar anions. In a cationic state, the present TTP donors are completely planar and have a more rigid molecular skeleton compared to BEDT-TTF, which has flexible and non-planar ethylenedithio groups. Such a high planarity, as well as a long molecular skeleton (twice as large as TTF), is electronically and sterically favorable to form a β-type donor packing.

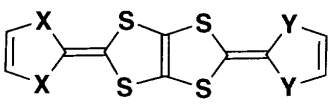

X = Y = S: TTP
X = S, Y = Se, ST-TTP
X = Y = Se, BDS-TTP

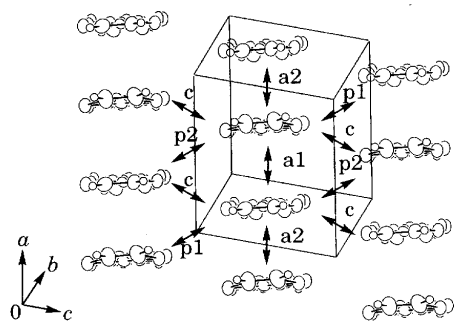

Figure 1. Donor sheet structure of $(BDS\text{-}TTP)_2AsF_6$.

V-M-2 Novel Oxygen Containing π-Electron Donors for Organic Metals: 2-(1,3-Dithiol-2-ylidene)-5-(pyran-4-ylidene)-1,3,4,6-tetrathiapentalenes

Yohji MISAKI *(Kyoto Univ. and IMS)*, **Hideki FUJIWARA** *(Kyoto Univ. and IMS)*, **Takashi MARUYAMA** *(Kyoto Univ.)*, **Masateru TANIGUCHI** *(Kyoto Univ.)*, **Tokio YAMABE** *(Kyoto Univ.)*, **Takehiko MORI** *(Tokyo Inst. Tech.)*, **Hatsumi MORI** *(ISTEC)* **and Shoji TANAKA** *(ISTEC)*

A bis-fused π-electron donor incorporating pyran-4-ylidene moiety, 2-(1,3-dithiol-2-ylidene)-5-(pyran-4-ylidene)-1,3,4,6-tetrathiapentalene (PDT-TTP), and its derivatives have been synthesized as donor components for organic conductors. The cyclic voltammograms of PDT-TTPs in benzonitrile are composed of two-pairs of single redox waves and one pair of two-electron one. The ethylendithio derivative ET-PDT have produced metallic salts with octahedral and liniear anions, which are stable down to 1.5-4.2 K. X-Ray structure analysis of the metallic PF_6^- salt of ET-PDT reveals that its composition is $(ET\text{-}PDT)_4PF_6(cn)$, where cn is 1-chloronaphthalene. The donors form conducting sheets, each of which is separated by the insulating layers composed of the anions and solvents. Two crystallographically independent ET-PDT molecules A and B form a face-to-face stack with four-folded period as A'ABB', in which the donors are stacked in a head-to-tail manner for molecules AA' and BB', and in a head-to-head manner for AB. The array of donors is close to that of an organic superconductor $\lambda\text{-}(BETS)_2GaCl_4$ (Figure 1). In the present salt, the head-to-tail overlap of the unsymmetrical π-electron framework of PDT-TTP prevents from an effective intrastack overlap. As a result, it has a strongly dimerized electronic structure along the stack direction in spite of its apparently uniform stack from the viewpoint of the interplanar distances. A tight-binding band calculations indicates it has an opened Fermi surfaces characteristic of quasi-one-dimensional metals.

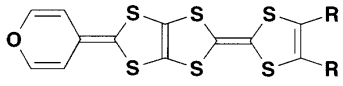

1a, R = H, PDT-TTP
1b, R = CO_2Me
1c, R = SMe
1d, 2R = $-S(CH_2)_2S-$, ET-PDT

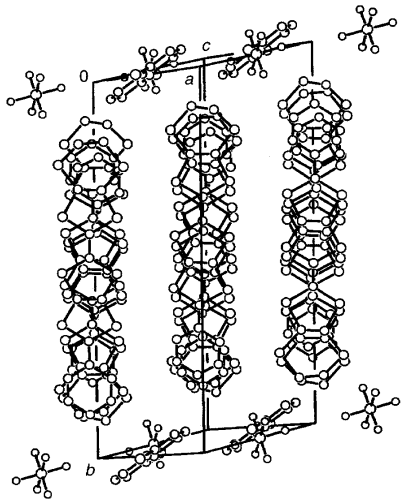

Figure 1. Crystal structure of $(ET\text{-}PDT)_4PF_6(cn)$.

V-M-3 Structures and Physical Properties of TMEO-ST-TTP Salts

Yohji MISAKI *(Kyoto Univ. and IMS)*, **Masateru TANIGUCHI** *(Kyoto Univ.)*, **Tadahiro KAIBUKI** *(Kyoto Univ.)*, **Koji TANAKA** *(Kyoto Univ.)*, **Tokio YAMABE** *(Kyoto Univ.)*, **Kazuyoshi TANAKA** *(Kyoto Univ.)*, **Kazuo TAKIMIYA** *(Hiroshima Univ.)*, **Atsushi MORIKAMI** *(Hiroshima Univ.)*, **Tetsuo OTSUBO** *(Hiroshima Univ.)* **and Takehiko MORI** *(Tokyo Inst. Tech.)*

A new donor TMEO-ST-TTP, where TMEO-ST-TTP is 2-[4,5-bis(methylthio)-1,3-diselenol-2-ylidene]-5-(4,5-ethylendioxy-1,3-dithiol-2-ylidene)-1,3,4,6-tetrathiapentalene, has been prepared. It affords highly conducting PF_6^- and AsF_6^- salts retaining metallic conductivity down to 4.2 K, while the TCNQ complex and ClO_4^- salt are low conductive semiconductors. X-Ray structure analysis of $(TMEO\text{-}ST\text{-}TTP)_2AsF_6$ reveals that this salt has the so-called β-type array of donors (Figure 1). A tight-binding band calculation suggests the present salt has a quasi one-dimensional Fermi surface opened along the stacking direction because the donors are dimerized in the stack.

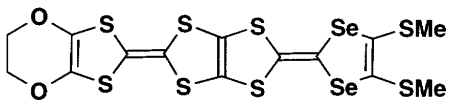

TMEO-ST-TTP

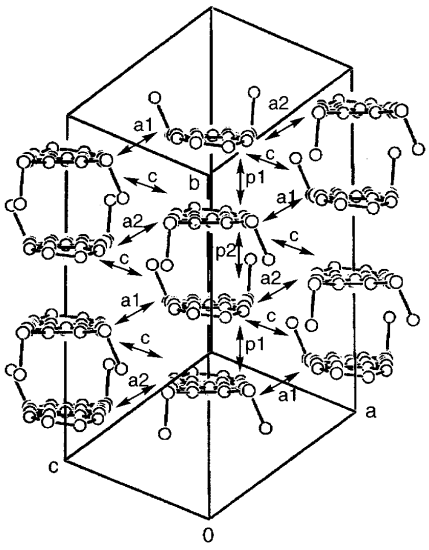

Figure 1. Donor sheet structure of $(TMEO\text{-}ST\text{-}TTP)_2AsF_6$.

V-M-4 Preparation and Properties of Gold Complexes with TTF-Dithiolato Ligands

Yohji MISAKI *(Kyoto Univ. and IMS)*, **Kazuyoshi TANAKA** *(Kyoto Univ.)* **and Klaus BECHGAAD** *(Risø National Lab.)*

A new family of metal complex with TTF-dithiolato ligands, $Au(dt)_2$ and $Au(tmdt)_2$, where dt and tmdt are 2-(1,3-dithiol-2-ylidene)- and 2-[4,5-bis(methylthio)-1,3-dithiol-2-ylidene]-1,3-dithiole-4,5-dithiolato, have been prepared. Cyclic voltammograms of tetrahexylammonium salts of $Au(dt)_2$ and $Au(tmdt)_2$ showed three and two pairs of irreversible waves, respectively. X-Ray structure analysis of $Bu_4N{\cdot}Au(dt)_2$ reveals that the $Au(dt)_2$ anion takes a slightly folded chair conformation with the dihedral angles of 8.6°. The neutral $Au(dt)_2$ and $Au(tmdt)_2$ exhibited high conductivity ($\sigma_{rt} = 10^0$ S cm^{-1}) on a compressed pellet, both of which showed semiconductive behavior with very low activation energies (E_a = 0.017-0.035 eV).

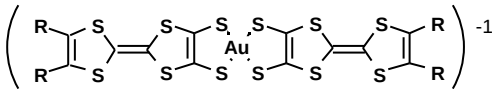

R'_4N^+

R = H, $(n\text{-}C_6H_{13})_4N{\cdot}Au(dt)_2$
R = SMe, $Bu_4N{\cdot}Au(tmdt)_2$

V-N Theoretical Study of the Electronic Structures of Weakly Bound Molecules

The electronic structures of weakly bound molecules such as van der Waals molecules are investigated by using sophisticated methods for electronic states, i.e., multi-reference single and double excitation configuration interaction (MRSDCI) and multi-reference coupled pair approximation (MRCPA) calculations.

V-N-1 Multi-Reference Coupled Pair Approximation (MRCPA) Calculations for the Ground State of the ArI_2 Complex

Eisaku MIYOSHI, Jun MAKI *(Hokkaido Univ.)*, **Takeshi NORO** *(Hokkaido Univ.)* **and Kiyoshi TANAKA** *(Hokkaido Univ.)*

[*J. Mol. Struct. Theochem* in press (1998)]

To investigate the relative stability of the T-shaped and linear isomers of the ArI_2 complex, multi-reference coupled pair approximation (MRCPA) and multi-reference single and double excitation configuration interaction (MRSDCI) calculations as well as single-reference CPA (SRCPA) and single-reference SDCI (SRSDCI) calculations were performed using relativistic model core potentials (MCPs) which included major relativistic effects. The localized natural orbitals (LNOs) set approach was used to calculate the correlation energy.

The T-shaped and linear isomers have almost the same binding energies. MRCPA calculations give a potential surface on which the T-shaped minimum is lower than the linear minimum by 9 cm^{-1}, which is in sharp contrast to those obtained by the SR approaches by Kunz *et al.*[1] who predicted that the linear isomer was more stable than the T-shaped isomer by 27, 18 and 13 cm^{-1} at the MP2, MP4 and CCSD(T) levels, respectively. Thus, the MR approach prefers the T-shaped isomer and is indispensable for investigating the relative stability of the linear and T-shaped isomers of halogen-rare gas van der Waals complexes.

Reference

1) C. F. Kunz, I. Burghardt and A. Hess, *J. Chem. Phys.* **109**, 359 (1998).

V-N-2 *Ab Initio* Study of the Ground and Excited States of ArHF

Tapas Kumar GHOSH, Eisaku MIYOSHI and Kiyoshi TANAKA *(Hokkaido Univ.)*

The class of van der Waals molecules involving the bonding between a rare gas atom and a hydrogen halide has gained intense impetus to both experimental and theoretical investigations because of its weakly intermolecular forces. In this study we have investigated the electronic structures of a van der Waals molecule, Ar-HF, to obtain the spectroscopic parameters and intermolecular potential energy surfaces for the ground $X\,^1\sum_g^+$ and excited $2\,^1\sum_g^+$ states. Calculations have been performed with a linear Ar-H-F structure. The dependence of both Ar-F and H-F distances have been studied. The excited $2\,^1\sum_g^+$ state is of ionic type (H^+F^-) and dissociates to a negative fluorine ion. This ,in turn, enlightens the photochemical reaction of the ionic excited HF with Ar correlating to the production of negative F ion:

$ArHF + h\nu \rightarrow Ar + (H^+F^-)^* \rightarrow (ArH^+)^* + F^-$.

V-N-3 *Ab Initio* Molecular Orbital Study of $Fe(CO)_n$ (n = 1, 2, and 3)

Hiroaki HONDA *(Hokkaido Univ.)*, **Takeshi NORO** *(Hokkaido Univ.)* **and Eisaku MIYOSHI**

Various unsaturated iron carbonyl complexes $Fe(CO)_n$ (n = 1 to 4) have been produced by the UV photolysis of iron pentacarbonyl $Fe(CO)_5$.[1] Among them the spectroscopic studies of the FeCO radical has been extensively performed from both experimental and theoretical points of view and there have been a few experimental spectroscopic constants of $Fe(CO)_2$ and $Fe(CO)_3$.

Although there have been published several theoretical studies for $Fe(CO)_2$ and $Fe(CO)_3$, there are few comprehensive studies for the change of bonding nature in the $Fe(CO)_n$ (n = 1 to 3) radicals. In this study we will investigate spectroscopic constants of the $Fe(CO)_n$ (n = 1 to 3) radicals by the use of *ab initio* calculations and discuss the change of the bonding nature through the donation and back-donation scheme in the radicals. Going from FeCO to $Fe(CO)_3$, the σ donation and π back-donation per CO decrease, which is consistent with the increase of vibrational frequencies of C-O stretch.

Reference

1) K. Tanaka, K. Sakaguchi and T. Tanaka, *J. Chem. Phys.* **106**, 2118 (1997).

V-O Molecular Dynamics Study Using Potentials by *Ab Initio* Molecular Orbital Calculations

Using potentials obtained by *ab initio* molecular orbital calculations, molecular dynamics calculations were performed to investigate physical properties of liquid mercury.

V-O-1 Molecular Dynamics Study of Liquid Mercury in the Density Region between Metal and Nonmetal

Tomonari SUMI *(Kyushu Univ.)*, **Eisaku MIYOSHI and Kiyoshi TANAKA** *(Hokkaido Univ.)*

We performed SDCI, SDCI(+Q), and CPA calculations for the ground $^1\sum_g^+$ state of Hg_2 incorporating the 5d and 6s electron correlations and major relativistic effects. The many-electron-excitation effect produces spectroscopic constants close to the experimental values. Although the metal-nonmetal (M-NM) transition can be explained as a simple band-crossing transition in one-electron theory, the many-electron-excitation effect is very important for describing the interaction between mercury atoms.

MD calculations for expanded liquid mercury were

performed using the potential energy curve of Hg_2, in the regions including the M-NM transition range. The volume (V) dependence of the thermal pressure coefficient, γ_v, and the internal pressure, P_0, estimated by the MD calculations agree well with experimental results. Thus, many-body interactions or the qualitative change in the form of interatomic interactions arising from density dependence are not necessarily essential to explain the behavior of the γ_v vs. V and the P_0 vs. V curves. The change of calculated pair distribution function between metallic and nonmetallic state qualitatively demonstrates the change of experimental ones. The temperature dependence of the isochoric electrical conductivity was estimated using interatomic distances obtained from the calculated pair distribution functions. It was shown that the increase of the isochoric electrical conductivity accompanying an increase in temperature can be realized through the increase of the density of states at the Fermi energy. In the preceding paper,[1] we reported that the MD calculations near the melting point using the potential curve of Hg_2 reproduce the cooperative motion corresponding to the collective short-wavelength excitations in the dynamic structure factor. These results suggest that pair-potential approximation using the potential curve of the dimeric molecule gives a good qualitative description of the metallic interatomic force for liquid mercury, and MD calculations using this approximation demonstrate the characteristic change of force fields between liquid metal and liquid semiconductor. However, the both γ_v vs. V and P_0 vs. V curves estimated by the MD calculations seem to deviate from the observed values slightly in the high-density metallic region. These differences between the observed and calculated values may be attributed to the lack of the many-body effects.

It has been pointed out[2] that the relative importance of three-body interactions compared with two-body interactions in the liquid-vapor critical range for mercury is larger than for other van der Waals molecules. The boiling point determined by the present MD calculations is much higher than the observed value. This higher temperature should be corrected by considering three-body effects, such as the Axilrod-Teller interaction, because the three-body dispersion forces are repulsive while the two-body dispersion force is a long-range attractive force. It is interesting to determine the liquid-vapor coexistence curve with pair-potential approximation using the potential energy curve of Hg_2 and to investigate the contribution of three-body effects to the liquid-vapor transition phenomena, especially in liquid-vapor critical range.

References

1) T. Sumi, E. Miyoshi, Y. Sakai and O. Matsuoka, *Phys. Rev. B* **57**, 914 (1998).
2) M. W. Pestak, R. E. Goldstein, M. W. Chan, J. R. de Bruyn, D. A. Balzarini and N.W. Ashcroft, *Phys. Rev. B* **36**, 599 (1987).

V-O-2 Molecular Dynamics Study for the Liquid-Vapor Coexistence Curve of Mercury

Tomonari SUMI *(Kyushu Univ.)* **and Eisaku MIYOSHI**

Critical behaviors in liquid-vapor coexistence curves of alkali metals such as Rb and Cs and of inert gases such as Ar and Xe and of mercury (Hg) have been shown to belong to different types of class.[1] The alkali metals and inert gases violate the particle-hole symmetry, which is valid for the universality class of three-dimensional Ising model, and the coexistence curves of alkali metals are extremely asymmetric.[1] It has been predicted that many-body interactions lead to the symmetry breaking in these fluids.[2] The coexistence curve of Hg is much more symmetric than that of the alkali metals and inert gases. We performed molecular dynamics (MD) calculations of fluid mercury using the potential energy curve of dimeric mercury obtained from ab initio molecular orbital calculations to determine the coexistence curve of mercury. Our MD calculations reproduced the symmetric coexistence curve of mercury.

References

1) F. Hensel, *J. Phys. C* **2**, SA33 (1990).
2) R.Goldstein and N.E. Aschcroft, *Phys. Rev. Lett.* **55**, 2164 (1985).

V-P Structures and Dynamics of Negatively-Charged Molecular Clusters

Negatively-charged molecular clusters continues to receive much attention as subjects for numerous theoretical and experimental investigations. The main interest has been focused on their fundamental properties concerning the electronic structures: i.e., how the aggregates of molecules bind an excess electron and how the electronic structures evolve with cluster size. Of particular interest are (1) the extent of charge localization/delocalization in the negatively-charged clusters, and (2) the existence of "electronic isomers" having different electronic structures. In our recent study, negative-ion photoelectron spectroscopy, in combination with *ab initio* calculations, have provided valuable information on the electronic properties of negatively-charged molecular clusters.

V-P-1 Formation of $N_3O_3^-$ anion in $(NO)_n^-$: Photoelectron Spectroscopy and *Ab Initio* Calculations

Tatsuya TSUKUDA *(Univ. Tokyo)***, Morihisa SAEKI, Lei ZHU and Takashi NAGATA**

[*Chem. Phys. Lett.* in press]

Anions of dimeric molecules often form tightly

bound species where the excess electron is delocalized to some extent over the dimer framework. For example, our recent photodetachment experiment has provided an evidence for a covalent $(CS_2)_2^-$ anion.[1)] In the present study, we have shown for the first time that anions of trimeric molecules can form covalent molecular anion. The photoelectron spectra of $(NO)_n^-$ ($1 \le n \le 7$) are recorded at a photon energy of 4.66 eV (Figure 1), and the vertical detachment energies (VDEs) are determined as a function of the cluster size. The VDE shows an abrupt increase from 2.93±0.05 eV at n = 2 to 3.70± 0.02 eV at n = 3. This large VDE shift is attributed to the formation of an $N_3O_3^-$ molecular anion, which acts as a core in the larger clusters; hence, the $(NO)_n^-$ clusters with $n \ge 3$ are well described as $N_3O_3^-\cdot(NO)_{n-3}$. *Ab initio* calculations are also performed at the MP2/6-31+G* level of theory. The calculations predict that the $N_3O_3^-$ anion has either normal or branched chain configuration shown in Figure 2.

Reference

1)T. Tsukuda, T. Hirose and T. Nagata, *Int. J. Mass Spectrum. & Ion Proc.* **171**, 273 (1997).

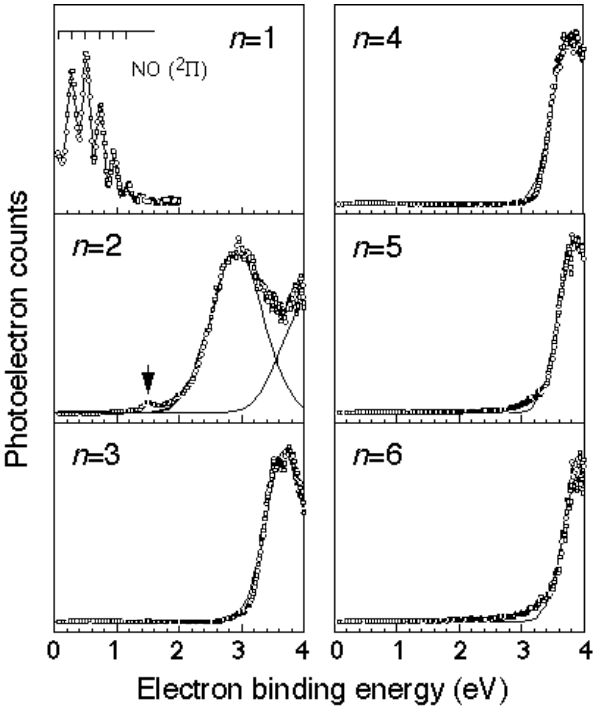

Figure 1. Photoelectron spectra of $(NO)_n^-$ with $1 \le n \le 6$. The open circles represent the experimental data. In the n = 1 spectrum the vibrational combs are shown for the ν_1 progression of NO. The best-fit Gaussian curves for $n \ge 3$ are shown by the solid lines.

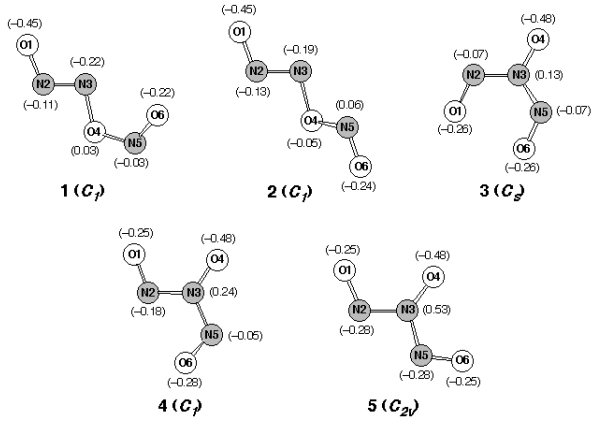

Figure 2. Optimized geometries of $N_3O_3^-$ obtained at the MP2/6-31+G* level. The shaded circles correspond to N atoms and open circles to O atoms. The numbers in parentheses indicate the net atomic charges.

V-P-2 Coexistence of Electronic Isomers in $[(CO_2)_nROH]^-$: Photoelectron Spectroscopy and *Ab Initio* Calculations

Tatsuya TSUKUDA *(Univ. Tokyo)*, **Morihisa SAEKI and Takashi NAGATA**

[*J. Chem. Phys.* submitted]

The electronic structures of $[(CO_2)_{n-1}ROH]^-$ (R = H, CH_3) have been investigated using negative-ion photoelectron spectroscopy. Analysis of the photoelectron band envelopes has revealed that spectra of $[(CO_2)_{n-1}H_2O]^-$ with size $3 \le n \le 5$ and $[(CO_2)_2CH_3OH]^-$ are characterized by two vertical detachment energies (VDE). In the photoelectron-depletion measurement,[1)] we have found that the low-VDE component of the $[(CO_2)_2ROH]^-$ photoelectron band can be selectively photodepleted, whereas the depletion is observed to be recovered to some extent in the case of $[(CO_2)_4H_2O]^-$. From these experimental findings, in conjunction with the theoretical results obtained in our MP2/6-31+G* calculations, we have drawn the following conclusions: (1) The electronic structures of $[(CO_2)_nROH]^-$ (R = H, CH_3) are categorized into two groups according to the extent of charge localization /delocalization: one formulated as $CO_2^-\cdot ROH(CO_2)_{n-2}$ and the other as $C_2O_4^-\cdot ROH(CO_2)_{n-3}$. These "electronic isomers" exhibit the VDE difference of ≈ 1 eV, which can be probed directly by negative-ion photoelectron spectroscopy; (2) The electronic isomers, $CO_2^-\cdot ROH(CO_2)_{n-2}$ and $C_2O_4^-\cdot ROH(CO_2)_{n-3}$, coexist in $[(CO_2)_{n-1}H_2O]^-$ with size $3 \le n \le 5$ and in $[(CO_2)_{n-1}CH_3OH]^-$. In the $[(CO_2)_2ROH]^-$ clusters the $CO_2^-\cdot ROH(CO_2) \leftrightarrow C_2O_4^-\cdot ROH$ interconversion is hindered by an insurmountable potential barrier along the isomerization pathway. Therefore, $CO_2^-\cdot ROH(CO_2)$ and $C_2O_4^-\cdot ROH$ coexist without interconversion (*static coexistence*). On the other hand, the $[(CO_2)_4H_2O]^-$ clusters occur with the $CO_2^-\cdot ROH(CO_2)_3 \leftrightarrow C_2O_4^-\cdot ROH(CO_2)_2$ interconversion (*dynamic coexistence*); (3) The occurrence of the dynamic coexistence implies that the $CO_2^-\cdot ROH(CO_2)_{n-2} \leftrightarrow C_2O_4^-\cdot ROH(CO_2)_{n-3}$ isomerization pathway, which is not opened in the smaller clusters,

becomes accessible in the larger analogues. A possible model for the isomerization is proposed, where the CO_2 neutrals surrounding the CO_2^-·ROH complex alternately take part in the formation of $C_2O_4^-$·ROH.

Reference

1)T. Tsukuda, M. A. Johnson and T. Nagata, *Chem. Phys. Lett.* **268**, 429 (1997).

V-P-3 Relaxation of Photoexcited $(C_6F_6)_n^-$ Using Time-Resolved Photoelectron Spectroscopy

Tatsuya TSUKUDA *(Univ. Tokyo)*, **Morihisa SAEKI and Takashi NAGATA**

Sub-ps time-resolved photoelectron spectroscopy was applied to probe the relaxation process of photo-excited $(C_6F_6)_n^-$ cluster anion. When $(C_6F_6)_n^-$ is photo-excited at ≈ 800 nm, photodissociation leading to the loss of one or two C_6F_6 molecules occurs competitively with the direct photodetachment. As the electronic excitation is possibly localized in the chromophore of $(C_6F_6)_n^-$, the conversion and dissipation of the electronic energy precede the evaporation of the C_6F_6 solvent:

$$\begin{array}{c}[C_6F_6^-(C_6F_6)_{n-1}] + h\nu \\ \downarrow \\ [C_6F_6^{-*}(C_6F_6)_{n-1}] \\ \downarrow \\ [C_6F_6^-(C_6F_6)_{n-1}]^{\dagger} \\ \downarrow \\ (C_6F_6)_m^- + (n\text{-}m)C_6F_6.\end{array}$$

In our experiment, the pump and probe pulses were generated by dividing the 790 nm output (390 fs) of a femtosecond laser system installed at the Laser Research Center for Molecular Science of IMS. The first pulse prepares the $(C_6F_6)_n^-$ in an electronically excited state, and the second pulse photodetaches the dissociating $(C_6F_6)_n^-$ clusters. While either pump or probe pulse itself detaches $(C_6F_6)_n^-$ to produce photoelectrons, additional photoelectron signals are observed when the pump and probe pulses are temporally overlapped. The signals appear around the kinetic energy of $2h\nu$ - VDE, where VDE represents the vertical detachment energy of the $(C_6F_6)_n^-$ clusters. The signal intensity decrease monotonically with the delay time Δt between the pump and probe laser pulses. The intensity vs Δt plots provide the characteristic decay time of ≈ 1.5 ps for the photoprepared electronic states of $(C_6F_6)_n^-$ with n = 3 and 4.

V-Q Millimeter-Wave Spectroscopy Combined with Pulsed-Jet Expansion Technique for the Detection of the Novel Unstable Species and the van der Waals Mode Transitions of Molecular Clusters

Molecular clusters have inherently low-frequency vibrations, so called van der Waals (vdW) vibrational modes, which are characteristic of the weakly bound complexes. The frequency of the vdW mode usually falls in the far-infrared region (30 - 300 cm^{-1}). However, if a cluster is extremely floppy, it sometimes falls in the submillimeter-wave (SMMW) region below 30 cm^{-1}.

The ArHCN cluster is a typical example which has extremely low-frequency vdW bending mode vibrations. Although the frequency of the vdW stretching is estimated to be 23.8 cm^{-1}, those for the bending vibrations are calculated to be as low as 4 - 7 cm^{-1}. Following the observation of the pure rotational spectra in the microwave region below 20 GHz, the vdW bending transitions of ArHCN have been measured in the millimeter-wave region near 180 GHz by molecular beam electric resonance optothermal spectroscopy (EROS).

In this project, a millimeter-wave absorption spectrometer combined with pulsed-jet expansion technique has been devised and applied to the direct observation of the rovibrational transitions of the vdW bending band of molecular clusters.

In the supersonic jet expansions short lived species can survive thanks to the collision-less environment and ultra low rotational as well as vibrational temperature. The millimeter-wave spectrometer combined with supersonic jet nozzle and glow discharge electrodes, as well as the UV excimer laser photolysis devices, also have been set up for the detection of novel unstable species, such as radicals, molecular ions, and ionic and radical clusters.

V-Q-1 Direct Absorption Observation of the van der Waals Bending Band of the ArDCN Cluster by Millimeter-Wave Spectroscopy Combined with Pulsed-Jet Expansion Technique

Stéphane BAILLEUX, Asao MIZOGUCHI, Kensuke HARADA, Tsuyoshi BABA *(Kyushu Univ.)*, **Mitsuaki SHIRASAKA** *(Kyushu Univ.)* **and Keiichi TANAKA** *(Kyushu Univ. and IMS)*

Millimeter-wave spectroscopy combined with a pulsed supersonic jet nozzle was applied to observe the absorption spectra of the van der Waals bending band of the ArDCN cluster in the frequency region 180 - 300 GHz. In total 53 rovibrational lines split into hyperfine structure due to nitrogen nucleus were observed and assigned to those for the $\sum_1$ - $\sum_0$ and $\prod_1$ - $\sum_0$ subbands of the j = 1 - 0 vdW fundamental bending band. The spectrum of the $Q(2)$ line of the $\prod_1$ - $\sum_0$ band observed at 196 GHz is shown in Figure 1.

The pure rotational spectrum in the ground $\sum_0$ state has been measured with the same spectrometer in the frequency region 40 - 71 GHz. The high-J transitions up

to J = 23 - 22 were observed and the molecular constants including the higher order centrifugal distortion constants in the ground state were derived.[1)]

The simultaneous analysis of the vdW bending mode transitions together with the pure rotational lines provided an accurate set of molecular constants, including the band origins, rotational constants, quadrupole coupling constants, and the Coriolis coupling constant between the $\sum_1$ and $\prod_1$ bending substates. Analysis of the hyperfine structure gives the *eqQ* values to be -3.1429, 0.8129, and 0.8022 MHz for the $\sum_0$, $\sum_1$, and $\prod_1$ states. The average angle $<\theta>$ between the principal axis of the cluster and the DCN part are derived to be 28, 62.5, and 62 degree, respectively. It means the average structure of the ArDCN cluster changes drastically by the excitation of the vdW bending mode from *linear* in the ground state to *T-shaped* in the first excited state. The band origins determined are unordinary higher, by 24.1 and 13.6 GHz, than those of the ArHCN species.[2)] Present molecular constants will be essential to improve the intermolecular potential surface between Ar and H(D)CN which is supposed to be double minimum corresponding to the linear and T-shape structures.[3)]

References

1)M. Shirasaka and K. Tanaka, *J. Mol. Spectrosc.* **185**, 189 (1997).
2)K. Uemura, A. Hara and K. Tanaka, *J. Chem. Phys.* **104**, 9747 (1996).
3)S. Drucker, A. L. Cooksy and W. Klemperer, *J. Chem. Phys.* **98**, 5158 (1993).

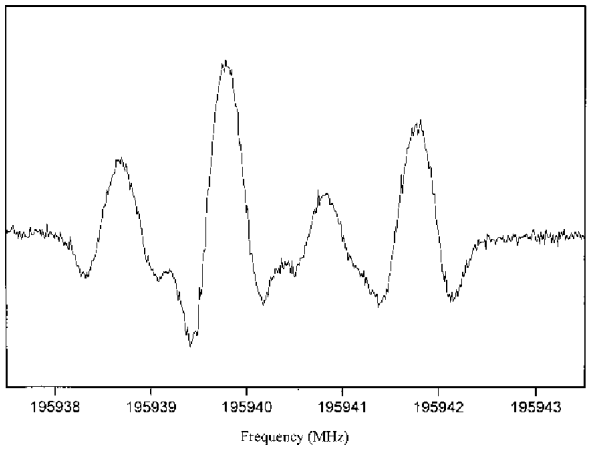

Figure 1. Hyperfine structure of the $Q(2)$ line of the $\prod_1 - \sum_0$ subband of the j = 1 - 0 vdW fundamental bending band of ArDCN.

V-Q-2 Millimeter-Wave Spectroscopy of the Iron Carbonyl Radical (FeCO) in the ν_2 State

Keiichi TANAKA *(Kyushu Univ. and IMS)*, **Mitsuhiro NAKAMURA** *(Kyushu Univ.)*, **Mitsuaki SHIRASAKA** *(Kyushu Univ.)* **and Takehiko TANAKA** *(Kyushu Univ.)*

The pure rotational spectrum of the iron carbonyl radical FeCO produced by a dc discharge of iron pentacarbonyl $Fe(CO)_5$ has been observed in the millimeter-wave (MMW) region. Seven rotational lines split into sextets, the electron spin components and Λ-type doubling components, were observed and assigned to those of the ν_2 bending vibrational state of FeCO. Although the symmetry of the ground electronic state is $^3\sum^-$, a large spin-orbit interaction constant A_{eff} = 14.0746 (57) GHz was obtained as well as the Λ-type doubling constants of o = -18.2899 (55) GHz, p = -355.36 (64) MHz and q = 9.5167 (69) MHz. The anomalously large fine structure splitting in the ν_2 state is explained by the vibronic interaction between the ν_2 bending vibrational state and the $^3\prod$ excited electronic state which is located very close (-6500 cm^{-1}) to the ground state.[1)]

The rotational and centrifugal distortion constants were determined to be B_0 = 4374.3908 (18) MHz and D_0 = 1.2497 (13) kHz. The spin-spin interaction constant and its higher order term are as large as λ_0 = 679.37 (29) GHz and λ_D = -454.8 (39) kHz, similar to those of the ground state. The spin-rotation interaction constant is γ_0 = -1180.0 (19) MHz, where the figures in parentheses are standard errors to be attached to the last digit.

Reference

1)K. Tanaka, M. Shirasaka and T. Tanaka, *J. Chem. Phys.* **106**, 6820 (1997)

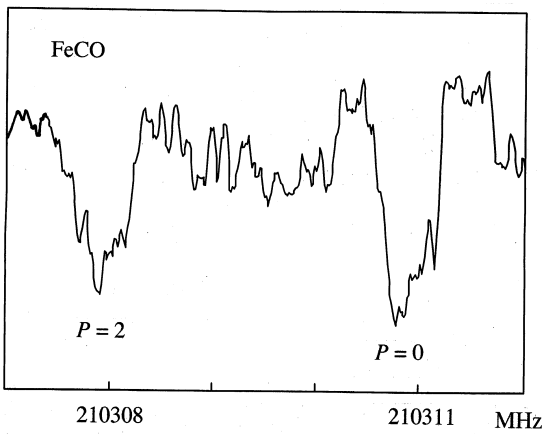

Figure 1. The Λ-type doubling component $P = 0^f$ and 2^f of the J = 24 ← 23 rotational transition of the FeCO radical in the ν_2 vibrational state.

V-R Ion-Molecule Reactions in the Troposphere

Ion chemistry in the troposphere is the most complicated among all level of earth's atmosphere because of the presence of a variety of trace compounds. We have been studying ion-molecule reactions in the troposphere by

investigating ion mobility distribution and its dependence on reaction time, pressure and temperature using an ion mobility spectrometer.[1,2] In order to confirm the ion-molecule reactions occurring in the troposphere, we designed high-resolution ion mobility/mass spectrometer which is capable of chemical identification of ion species forming ion peaks in mobility spectra. Using this spectrometer, we will investigate the ion processes in conditioned laboratory air as well as in natural air.

References

1)K. Nagato and T. Ogawa, *J. Geophys. Res.* **103**, 13917 (1998)
2)K. Nagato, D. J. Tanner, H. R. Friedli and F. L. Eisele, *J. Geophys. Res.* submitted.

V-R-1 Development of High-Resolution Ion Mobility/Mass Spectrometer for the Study of Ion-Molecule Reactions in the Troposphere

Kenkichi NAGATO

We have designed a high-resolution ion mobility/mass spectrometer which can make simultaneous measurements of mobility and mass spectra of cluster ions generated by ion-molecule reactions under atmospheric pressure. The spectrometer consists of a drift tube, a mass analyzer, and an interface chamber between the drift tube and the mass analyzer. Ions to be analyzed are generated by irradiation of sample air with an americium source and enter into the drift tube. In the drift tube, ions experience a chain of ion-molecule reactions with trace species in the sample air and are separated into different ion groups according to their mobility by an uniform electric field. The length of the drift tube can be varied up to about 40 cm, which allows measurements of ions aged for about 5 s. Ions are introduced through an aperture (100-200 μm) into the interface chamber which is differentially pumped by a rotary pump (800 l/min) and a turbo molecular pump (230 l/s). Ions are finally mass-analyzed by a quadrupole mass filter in a detection chamber which is pumped by a 10" diffusion pump. A preliminary experiment with this spectrometer is underway.